show 13-fold enrichment of CNVs over the average genomic coverage in a reference assembly [23]. Therefore, CNVs or structural variations are recognized as significant contributors to human genetic disease and disease susceptibility [24].

In the search for susceptibility gene(s) for T2DM genes, we recruited a panel of 100 early-onset Japanese T2DM patients (onset age <35 years) and 100 controls, and performed CNV analysis in the whole genome using the deCODE-Illumina CNV370K BeadChip which focuses on the CNV-rich region of the human genome, followed by validation and characterization using an Agilent region-targeted high-density custom-made oligonucleotide tiling microarray. We found frequent copy number losses within the 1.3-Mb subtelomeric region in a substantial portion of early-onset Japanese T2DM patients. This region surrounds the genome gap in 4p16.3, which is rich in multiple low copy repeats.

2. Materials and Methods

2.1. Subjects. We considered that the early onset of T2DM reflects the presence of more genetic factors rather than environmental factors. Therefore, we adopted young-onset diabetic patients as case subjects. We studied 100 unrelated Japanese T2DM patients who developed T2DM before 35 years of age. They were recruited at Tohoku University Hospital and affiliated hospitals and medical clinics. Diabetes was diagnosed using the WHO criteria. Type 1 diabetes mellitus was excluded judged from clinical features and existence of anti-GAD (glutamic acid decarboxylase) antibodies or anti-IA-2 (insulinoma-associated antigen-2) antibodies. Patients with diabetes mellitus due to hepatic disease, pancreatic disease, other endocrinological disease, or mitochondrial DNA mutation, or drug-induced diabetes were excluded, judged from laboratory data and clinical history.

We also studied 100 nondiabetic control subjects, using the following criteria: 60 or more years of age, no prior diagnosis of diabetes mellitus, HbA1c less than 6.4% (where HbA1c (%) was estimated as an NGSP (National Glycohemoglobin Standardization Program) equivalent value (%) calculated by the formula HbA1c (%) = HbA1c (JDS: Japan Diabetes Society value) (%) + 0.4%, considering the relational expression of HbA1c (JDS) (%) measured by the previous Japanese standard substance and measurement methods for HbA1c (NGSP) [25] and no family history of T2DM within third-degree relatives, in order to exclude subjects who were more likely to develop diabetes later.

Clinical features available from 100 early-onset T2DM patients and 100 controls are shown in (see Table S1 in Supplementary Material available online at doi: 10.1155/2011/498460). In addition, clinical features of the 13 early-onset T2DM patients with copy number losses in 4p16.3 are shown separately in Supplementary Table S2 and Supplementary Table S3 in comparison with the rest of 100 early-onset T2DM patients without copy number loss ($n = 87$).

Genetic analysis of human subjects was approved by the ethics committee of Tohoku University Graduate School of Medicine. Appropriate informed consent was obtained from all the subjects examined.

2.2. Screening with Whole-Genome CNV BeadChip. We screened the whole genome by CNV analysis using the deCODE-Illumina CNV370K BeadChip (Illumina Infinium system, deCODE genetics, Inc., Iceland), which, in addition to Hap300 SNP marker contents, has CNV probes designed to target the CNV-rich region of the whole genome. The CNV part of the platform consists of probes covering CNV-rich regions of the genome, such as megasatellites (tandem repeats >500 bp), duplicons (region flanked by highly homologous segmental duplication >1 kb), unSNPable regions (>15 kb gaps in HapMap SNP map, and 5–15 kb gaps with >2SNPs with Hardy-Weinberg failure), and CNVs registered in the Database of Genomic Variants. The CNV part of probe content consists of 15,559 CNV segments covering 190 Mb, or 6% of the human genome. The platform has been tested in 4000 Icelandic and HapMap samples.

Data analysis of the deCODE-Illumina CNV chip was carried out using DosageMiner software developed by deCODE genetics, and loss/gain analysis consisted of the following four steps; (1) intensity normalization and GC content correction, (2) removal of batch effects using principal component analysis, (3) calling of clusters using a Gaussian mixture model, and (4) determination of CNV type using graphical constraints. In brief, CNVs were identified when CNV events stood out in the data, as all sample intensities for CNV probes should be increased or decreased relative to neighboring probes that are not in a CNV region. To determine deviations in signal intensity we started by normalizing the intensities. The normalized intensities for each color channel were determined by an equation and fit formula developed by deCODE genetics. A stretch with occurrence of more than one marker showing abnormality in the copy number in a consecutive stretch in the genome is considered more likely to be evidence of deletion or gain [26]. We display Supplementary Table to present raw data, that is, $\log_2$ ratio measured at each probe for every individual. Raw data at screening step via deCODE/Illumina beads chip for all probes on chromosome 4p is shown in Supplementary Table S4.

2.3. High-Density Custom-Made Oligonucleotide Tiling Microarray Analysis. DNA samples from 13 early-onset T2DM patients and 15 control individuals were subjected to Agilent's high-density custom-made oligonucleotide tiling microarray analysis based on an array comparative genomic hybridization (aCGH) assay. We fabricated a custom-designed microarray targeted to a 1.3-Mb genome region in the subtelomere at 4p16.3 (Chr. 4: 550,000-1,850,000 (NCBI Build 36.1, hg18)) according to previously described methods [27, 28]. In brief, we used the Agilent website (http://earray.chem.agilent.com/earray/) to select and design our custom tiling array; the array consisted of probes 60-mer in size (Agilent Technologies, Santa Clara, CA).

Tiling-aCGH experiments were performed essentially as described previously [29]. In brief, test and reference (NA19000, a Japanese male from HapMap project) genomic

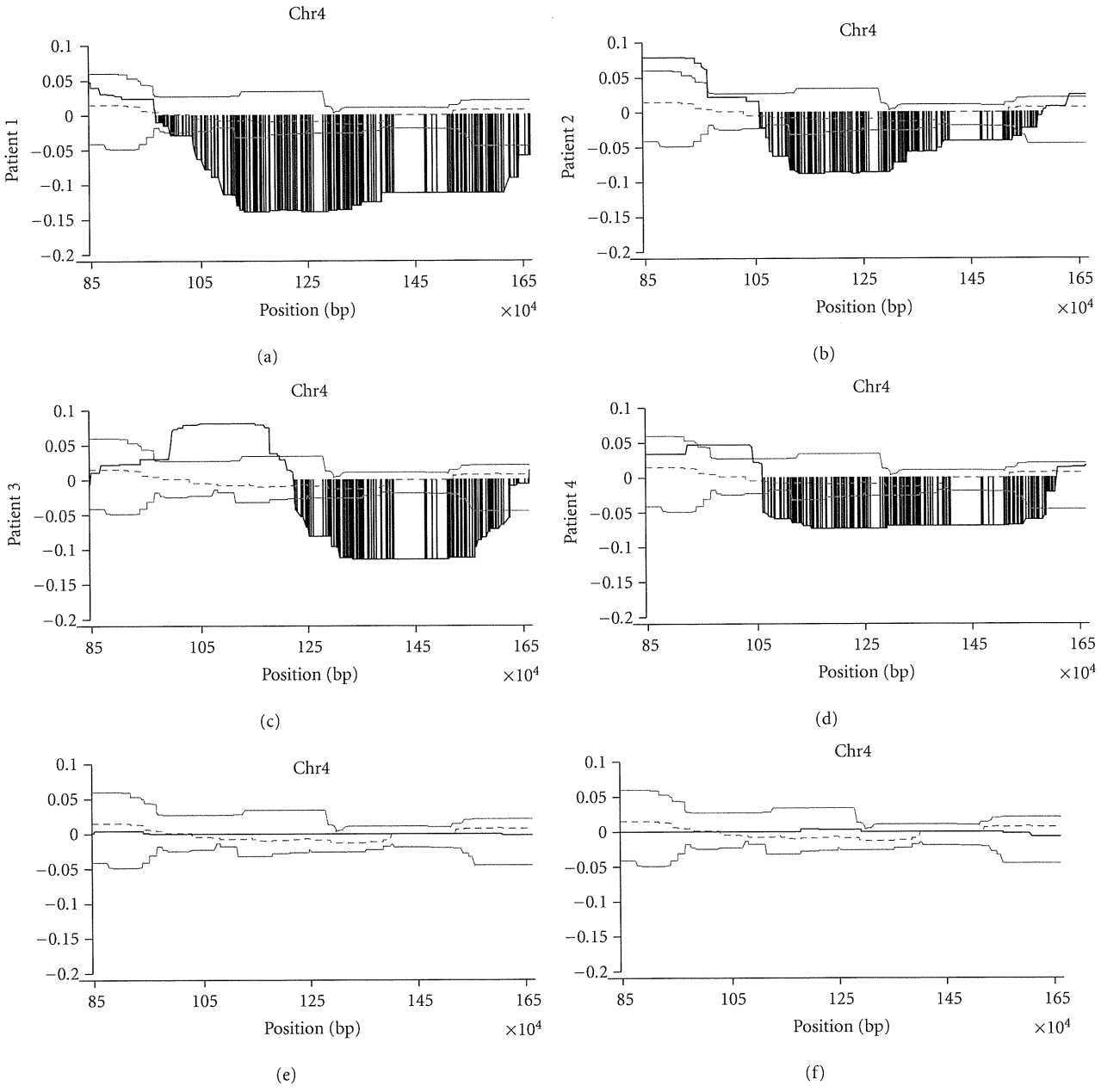

FIGURE 2: Detailed structure of copy number loss of 1.3-Mb 4p16.3 subtelomeric region resolved by high-density tiling microarray. Log_2 ratio (y-axis) was plotted using moving average along the genome position (x-axis). Four representative early-onset T2DM patients are shown as Figures 2(a), 2(b), 2(c), and 2(d), patient 1, 2, 3, and 4, respectively. For comparison, log_2 ratio of the region of two healthy normal individuals is also displayed as Figures 2(e) and 2(f). Dark line represents copy number plot along the genome. Two light lines indicate normal range of average log_2 ratios for probes among normal individuals. Dotted line shows median of average log_2 ratio among normal individuals. Copy number losses are displayed as gray vertical bar. We defined two copy number classes, that is, "unchanged copy number" and "copy number loss." "Unchanged copy number" was defined when the log_2 ratio stays within the mean ± 1 SD distribution among the normal population. "Copy number loss" was called when the downward-deviation of log_2 ratios exceeded a threshold of 1 SD from the median probe ratio.

DNAs (250 ng per sample) were fluorescently labeled with Cy5 (test) and Cy3 (reference) with a ULS Labeling Kit (Agilent Technologies).

For each sample, respective labeling reactions were mixed and then separated prior to hybridizing to each of the arrays. Labeled test and reference DNAs were combined, denatured, preannealed with Cot-1 DNA (Invitrogen) and blocking agent, and then hybridized to the arrays for 24 hr in a rotating oven at 65°C and 20 rpm (Agilent Technologies). After hybridization and washes, the arrays were scanned at 3 μm resolution with an Agilent G2505C scanner. Images were analyzed with Feature Extraction Software 10.7.3.1 (Agilent Technologies), with the CGH_107_Sep09 protocol for background subtraction and normalization. Detection

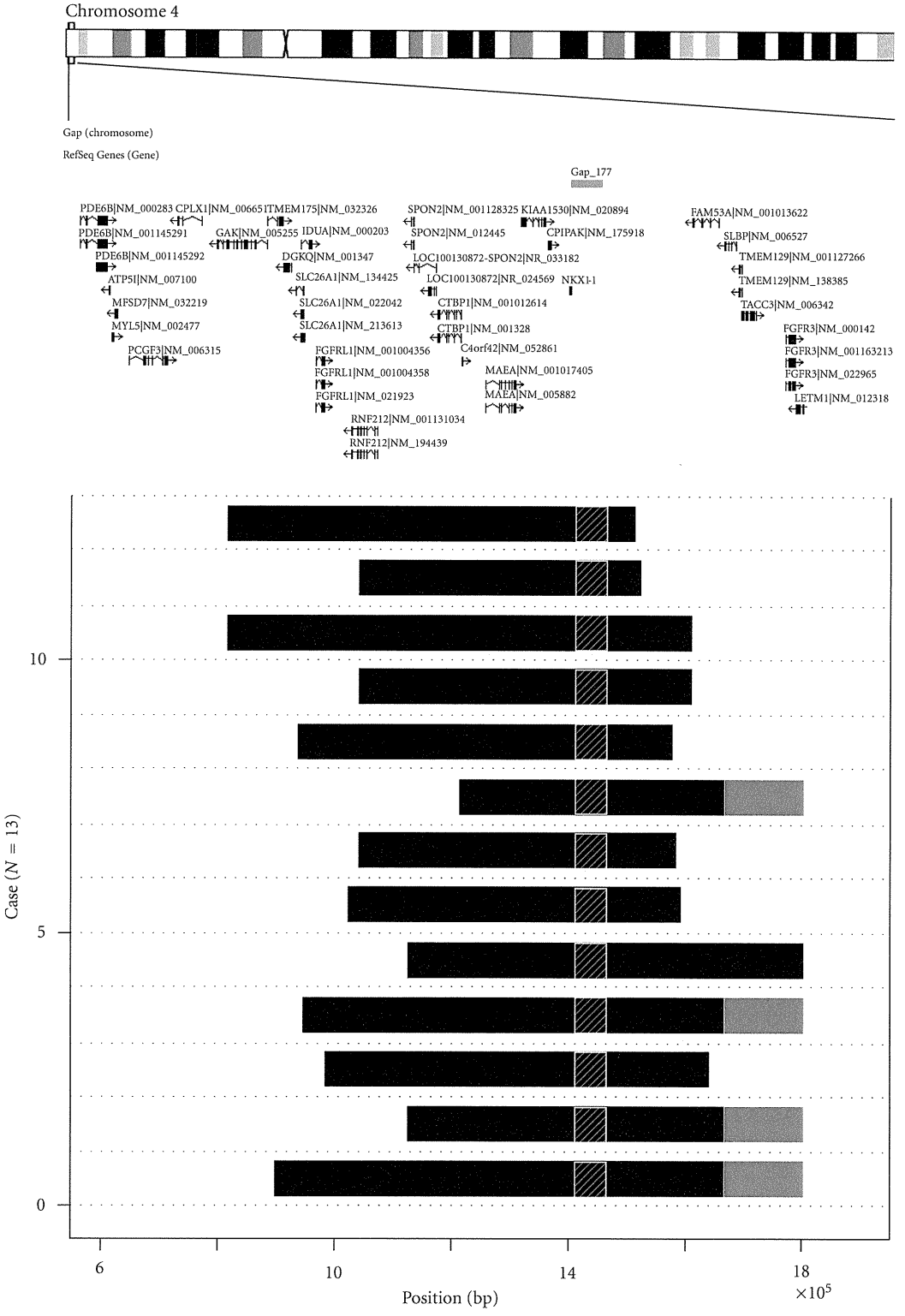

FIGURE 3: The extent of copy number losses within 1.3-Mb 4p16.3 subtelomeric region in 13 early-onset T2DM patients revealed by high-density oligonucleotide tiling microarray. Dark horizontal bars represent extent of copy number loss region in each patient revealed by Agilent custom tiling array. Genome structure of the 13 patients is aligned as horizontal bars from genome position 550,000 (left) to position 1,850,000 (right). Hatched region at position 1,423,147–1,478,646 represents genome gap-177 region. Gray regions represent proximal ends of stretch where copy number status was not inferred due to presence of multiple low copy repeats. Upper map shows ideogram of chromosome 4 and the positions of putative genes in 4p16.3 region described in Database of Genomic Variants (http://projects.tcag.ca/variation/). Position is given relative to NCBI Build 35 for the chromosome 4.

of abnormal copy number, losses, and gains, in a complex multicopy variable region by high-density tiling array was accessed by deviation of probe $\log_2$ ratios that exceeded a threshold of 1 SD from the median probe ratio, according to procedures described previously [29–31]. We defined two copy number classes, that is, "unchanged copy number" and "copy number loss." "Unchanged copy number" was defined when the $\log_2$ ratio stays within the mean ± 1 SD distribution among the normal population. "Copy number loss" was called when the downward-deviation of $\log_2$ ratios exceeded a threshold of 1 SD from the median probe ratio. Raw data, that is, $\log_2$ratio measured at each probe for every individual obtained by high-density custom-made tilling array analysis is shown in Supplementary Table S5.

3. Results

In searching for CNVs associated with early-onset T2DM, we screened the whole genome by CNV analysis using the deCODE-Illumina CNV370K BeadChip in 100 early-onset Japanese T2DM patients and 100 controls. We found four CNVs that fulfilled our screening criteria: (1) reliable CNV (size over 50-Kb, consisting of over 50 consecutive probes), (2) the association being statistically significant by Fisher's exact test which was accompanied by Bonferroni's correction. Four candidate CNV that fulfilled the criteria; that is, CNV on 4p16.3 ($P = 6.75 \times 10^{-3}$ by Fisher's exact test, $P < .05$ after Bonferroni's correction), CNV on 16p13.3 ($P = 3.44 \times 10^{-4}$ by Fisher's exact test, $P < .05$ after Bonferroni's correction), CNV on 16q24.3 ($P = 9.65 \times 10^{-3}$ by Fisher's exact test, $P < .05$ after Bonferroni's correction), and CNV on 19p 13.3 ($P = 1.61 \times 10^{-4}$ by Fisher's exact test, $P < .05$ after Bonferroni's correction). Of these CNVs listed, the CNV on 4p16.3 was intriguingly found to be located right on the genome gap-177 region on 4p subtelomere. At this candidate CNV on 4p16.3, 13 out of 100 T2DM patients displayed CN-loss around this CNV marker, compared with 1 out of 100 control samples. Because of its unique overlap with genome gap structure, we focused on this CNV region for further analysis.

Figure 1 shows the pattern of alterations in copy number loss observed among the 100 early-onset Japanese 2DM patients. Thirteen patients displayed copy number losses around the gap in the 4p16.3 subtelomere whereas only one of 100 control samples showed copy number losses in this region. The association was statistically significant by Fisher's exact test ($P = 6.75 \times 10^{-3}$, OR = 14.7, 95% confidence interval 3.02–72.3). We observed two copy number classes, that is, "unchanged copy number" and "copy number loss" at 1.3-Mb region of chromosome 4p16.3 in our diabetic or control populations. The latter was found frequently observed among early-onset T2DM patients at the 4p16.3 subtelomere. The position, length, or pattern of deletion between one copy number loss in control and 13 copy number losses in T2DM patients were not apparently distinct, although the case number is too small to draw meaningful conclusion.

To verify the CNV BeadChip results, we analyzed copy number changes along the 1.3-Mb region in the subtelomere surrounding the genome gap of 4p16.3 using a high-density custom-made oligonucleotide tiling microarray. We used peripheral blood DNA of the 13 early-onset T2DM patients, identified, and 15 control healthy individuals. Again, we found frequent copy number losses in regions around the genome gap in all the 13 early-onset T2DM patients, whereas none of 15 healthy individuals showed copy number losses.

Figure 2 shows detailed structure of copy number losses in four representative early-onset Japanese T2DM patients with copy number losses, in the 1.3-Mb region in the subtelomere (patients 1, 2, 3, 4; in Figures 2(a), 2(b), 2(c), and 2(d), resp.). Individual copy number plots using moving average (y-axis) versus distance along the chromosome (x-axis) are shown. As a comparison, copy number plots of healthy individuals who did not exhibit copy number alterations in the region are also shown (Figures 2(e) and 2(f)).

Figure 3 shows genomic copy number losses in all the 13 early-onset T2DM patients. High-density tiling custom-made microarray showed segmental losses in the subtelomeric region of 4p16.3 in all the 13 patients. Genomic copy number losses in these patients were clustered around a gap region in the 4p16.3 subtelomeric region.

4. Discussion

Our initial genome-wide screening with deCODE-Illumina CNV370K BeadChip for association with early-onset T2DM revealed losses in the subtelomeric region of 4p16.3. Subsequent high-density custom-made oligonucleotide tiling microarray verified copy number losses in this region.

It is worthy to note that most patients with copy number losses were treated with insulin injection. Urine C-peptide reactivity was not significantly different between the two groups, and only few patients underwent glucagon challenge test, thus, the data are too limited to infer the function of insulin secretion. We did not observe significant differences between two groups as to age of onset, body mass index, postprandial plasma glucose levels, or HbA1c levels. Fasting immunoreactive insulin levels were examined in 5 patients with copy number losses and 14 patients without copy number loss. HOMA-R in the former patients was 6.1 ± 6.8 (mean ± SD) and that in the latter patients was 5.5 ± 6.0 (mean ± SD); these values were not significantly different. Incidence of dyslipidemia, hypertension, diabetic retinopathy, nephropathy, or neuropathy was not different between the two groups (Supplementary Tables S2, S3). Further investigation of a large panel of patients would be necessary to clarify any clinical differences that might be present between the two groups.

The current map of CNV in the human genome reported in the existing databases is far from complete [32]. Increasing numbers of CNVs have recently been identified around repetitive sequences such as segmental duplications or low copy repeats. In fact, these repeat-rich regions were found to be 13-fold enriched in CNV over the average genomic coverage in the reference assembly [23]. Probes for conventional genome-wide SNP genotyping platforms are likely to be underrepresented; that is, only 25% and 40% of CNV are

Table 1: Putative genes located within 1.3-Mb region in 4p16.3 subtelomere.

Start	End	Cytogenetic location	Symbol	Description	Model evidence
609,373	654,571	4p16.3	PDE6B	Phosphodiesterase 6B, cGMP-specific, rod, beta (congenital stationary night blindness 3, autosomal dominant)	Best RefSeq
656,225	658,122	4p16.3	ATP5I	ATP synthase, H+ transporting, mitochondrial F0 complex, subunit E	Best RefSeq
661,711	665,817	4p16.3	MYL5	Myosin, light chain 5, regulatory	Best RefSeq
665,618	672,973	4p16.3	MFSD7	Major facilitator superfamily domain containing 7	mRNA
689,573	754,428	4p16.3	PCGF3	Polycomb group ring finger 3	Best RefSeq
719,829	721,544	4p16.3	LOC100128084	Hypothetical protein LOC100128084	mRNA
764,588	765,632	4p16.3	LOC100129917	Hypothetical protein LOC100129917	mRNA
768,745	809,945	4p16.3	CPLX1	Complexin 1	mRNA
833,065	916,174	4p16.3	GAK	Cyclin G associated kinase	mRNA
916,262	942,444	4p16.3	TMEM175	Transmembrane protein 175	Best RefSeq
942,675	957,344	4p16.3	DGKQ	Diacylglycerol kinase, theta 110 kDa	Best RefSeq
962,861	977,224	4p16.3	SLC26A1	Solute carrier family 26 (sulfate transporter), member 1	Best RefSeq
970,785	988,317	4p16.3	IDUA	Iduronidase, alpha-L-	mRNA
995,610	1,010,686	4p16.3	FGFRL1	Fibroblast growth factor receptor-like 1	Best RefSeq
1,044,654	1,045,386	4p16.3	LOC100132787	Hypothetical protein LOC100132787	mRNA
1,055,269	1,097,350	4p16.3	RNF212	Ring finger protein 212	Best RefSeq
1,116,050	1,129,814	4p16.3	LOC100133135	Hypothetical protein LOC100133135	Protein
1,135,541	1,135,957	4p16.3	FLJ35816	FLJ35816 protein	Protein
1,149,293	1,149,712	4p16.3	LOC100131106	Hypothetical protein LOC100131106	Protein
1,150,723	1,156,597	4p16.3	SPON2	Spondin 2, extracellular matrix protein	Best RefSeq
1,184,431	1,185,198	4p16.3	LOC100130872	Hypothetical protein LOC100130872	mRNA
1,195,228	1,232,908	4p16.3	CTBP1	C-terminal binding protein 1	Best RefSeq
1,234,177	1,236,616	4p16.3	C4orf42	Chromosome 4 open reading frame 42	Best RefSeq
1,273,672	1,323,925	4p16.3	MAEA	Macrophage erythroblast attacher	Best RefSeq
1,331,104	1,371,732	4p16.3	KIAA1530	KIAA1530	mRNA
1,375,340	1,379,782	4p16.3	CRIPAK	Cysteine-rich PAK1 inhibitor	mRNA
1,380,072	1,392,453	4p16.3	NKX1-1	NK1 homeobox 1	Protein
1,484,196	1,519,086	4p16.3	LOC100133199	Similar to RE32881p	mRNA
1,611,605	1,655,516	4p16.3	FAM53A	Family with sequence similarity 53, member A	Best RefSeq
1,664,325	1,683,828	4p16.3	SLBP	Stem-loop (histone) binding protein	Best RefSeq
1,687,477	1,692,882	4p16.3	TMEM129	Transmembrane protein 129	Best RefSeq
1,693,062	1,716,696	4p16.3	TACC3	Transforming, acidic coiled-coil containing protein 3	Best RefSeq
1,765,421	1,780,396	4p16.3	FGFR3	Fibroblast growth factor receptor 3 (achondroplasia, thanatophoric dwarfism)	Best RefSeq
1,784,558	1,827,772	4p16.3	LETM1	Leucine zipper-EF-hand containing transmembrane protein 1	Best RefSeq

covered by the HumanHap300 and HumanHap550 platform, respectively [23]. These recent findings may partly explain why earlier genome-wide association studies for CNVs in the T2DM population failed to detect CNV loci being strongly associated with T2DM [20, 21, 33, 34].

We found copy number losses among early-onset Japanese T2DM patients in a region surrounding a genome gap (gap-177) in the subtelomere of chromosome 4p16.3. The physical map of the human genome still contains a significant number of genome gaps; over 300 gaps still remain in the human draft genome sequence [35] that are considered inaccessible by most existing genotyping and sequencing technologies [36]. These gap regions are estimated to harbor ~1000 genes, which comprise approximately 5% of

the human genome (~200 Mb). In particular, they are abundant in subtelomeres and pericentromeric regions of chromosomes [37, 38]. Some of these gaps are thought to be susceptible sites for mediating meiotic recombination and are also susceptibility sites for break points for deletions [39, 40].

Many CNVs were recently identified in repeat-rich regions [41], which are predisposed to the generation of deletion/duplication events [22]. It is intriguing to note that the locus-specific mutation rates for CNV or structural rearrangements were estimated to be between 10^{-6} and 10^{-4}: two to four orders of magnitude greater than nucleotide-specific rates for base substitutions or point mutations [19].

The deleted CNV region found in the present study and its flanking region contained 34 genes (Table 1). Gene(s) in this region may predispose to T2DM.

Genes involved in the glucose-induced insulin secretion cascade of pancreatic beta-cells are located in the region, such as ATP5I (ATP synthase, H^+ transporting, mitochondrial F_0 complex, subunit E) [42, 43], CPLX1 (complexin 1) [44, 45], GAK (cyclin G associated kinase) in association with CDK5 (cyclin-dependent protein kinases 5) [46–50], and CRIPAK (cysteine-rich PAK1 inhibitor), which is a negative regulator of PAK1 (p21 protein (Cdc42/Rac-) activated kinase 1) [51, 52].

FGFR3 (fibroblast growth factor receptor 3) and FGFRL1 (fibroblast growth factor receptor-like 1) are suggested to be involved in pancreatic development and differentiation [53–56]. TACC3 (transforming, acidic coiled-coil containing protein 3) may be involved in embryonic development including the pancreas [57, 58].

CTBP1 (C-terminal binding protein 1) and MAEA (macrophage erythroblast attacher) have effects on adipose tissue functions [59, 60], which may lead to insulin resistance. NKX1-1(NK1 homeobox 1) may cause insulin resistance with a function in the maintenance of energy homeostasis [61].

Recently, through whole-genome screening of a copy number variation using a CNV BeadChip and real-time quantitative polymerase chain reaction (qPCR), Kato et al. identified a segmental copy number gain within the 40-kb region on 10p15.3 subtelomere in patients of sporadic amyotrophic lateral sclerosis (SALS) [62]. They demonstrated the copy number gain in 46 out of 83 SALS patients, as compared with 10 out of 99 controls. The copy number gain region they identified is rather small (40-kb) and harbored two genes encoding isopentenyl diphosphate isomerase 1 (IDI1) and IDI2. Thus, they suggested the copy number gain in the region of these genes may play a significant role in the pathogenesis of SALS. The present study share a similar genome abnormality in that we found frequent copy number alterations in subtelomere region among sporadic adult-onset disease of unknown cause. The copy number alterations we identified here in early-onset T2DM were copy number losses on different chromosome subtelomere (4p16.3) and the size is rather large (up to 1.3-Mb). In our case, we suspect that multiple genes in the region may be involved in diabetes pathogenesis through impairments caused by copy number losses.

5. Conclusion

These results suggested that copy number losses of the candidate genes in the deleted region surrounding the genome gap in 4p16.3 may play significant roles in the etiology of T2DM. Further functional study, as well as investigation of 4p16.3 loss in a large panel of early-onset T2DM patients in different ethnic populations and geographical regions, is warranted.

Acknowledgment

This paper was supported by a Grant-in-Aid for Scientific Research to Y. Oka (H19-genome-005) from the Ministry of Health, Labor, and Welfare of Japan, and was also supported by a grant from the Global-COE Programs for "Network Medicine" to Y. Oka and H. Katagiri from the Ministry of Education, Culture, Sports, Science, and Technology of Japan.

References

[1] T. M. Frayling, J. C. Evans, M. P. Bulman et al., "beta-cell genes and diabetes: molecular and clinical characterization of mutations in transcription factors," *Diabetes*, vol. 50, supplement 1, pp. S94–S100, 2001.

[2] J. M. van den Ouweland, H. H. Lemkes, W. Ruitenbeek et al., "Mutation in mitochondrial tRNA(Leu)(UUR) gene in a large pedigree with maternally transmitted type II diabetes mellitus and deafness," *Nature Genetics*, vol. 1, no. 5, pp. 368–371, 1992.

[3] Y. Oka, H. Katagiri, Y. Yazaki, T. Murase, and T. Kobayashi, "Mitochondrial gene mutation in islet-cell-antibody-positive patients who were initially non-insulin-dependent diabetics," *The Lancet*, vol. 342, no. 8870, pp. 527–528, 1993.

[4] H. Inoue, Y. Tanizawa, J. Wasson et al., "A gene encoding a transmembrane protein is mutated in patients with diabetes mellitus and optic atrophy (Wolfram syndrome)," *Nature Genetics*, vol. 20, no. 2, pp. 143–148, 1998.

[5] J. Kaprio, J. Tuomilehto, M. Koskenvuo et al., "Concordance for Type 1 (insulin-dependent) and Type 2 (non-insulin-dependent) diabetes mellitus in a population-based cohort of twins in Finland," *Diabetologia*, vol. 35, no. 11, pp. 1060–1067, 1992.

[6] P. Poulsen, K. O. Kyvik, A. Vaag, and H. Beck-Nielsen, "Heritability of type II (non-insulin-dependent) diabetes mellitus and abnormal glucose tolerance—a population-based twin study," *Diabetologia*, vol. 42, no. 2, pp. 139–145, 1999.

[7] J. B. Meigs, L. A. Cupples, and P. W. Wilson, "Parental transmission of type 2 diabetes: the Framingham Offspring Study," *Diabetes*, vol. 49, no. 12, pp. 2201–2207, 2000.

[8] C. F. Weijnen, S. S. Rich, J. B. Meigs, A. S. Krolewski, and J. H. Warram, "Risk of diabetes in siblings of index cases with Type 2 diabetes: implications for genetic studies," *Diabetic Medicine*, vol. 19, no. 1, pp. 41–50, 2002.

[9] S. F. Grant, G. Thorleifsson, I. Reynisdottir et al., "Variant of transcription factor 7-like 2 (TCF7L2) gene confers risk of type 2 diabetes," *Nature Genetics*, vol. 38, no. 3, pp. 320–323, 2006.

[10] H. Unoki, A. Takahashi, T. Kawaguchi et al., "SNPs in KCNQ1 are associated with susceptibility to type 2 diabetes in East Asian and European populations," *Nature Genetics*, vol. 40, no. 9, pp. 1098–1102, 2008.

[11] K. Yasuda, K. Miyake, Y. Horikawa et al., "Variants in KCNQ1 are associated with susceptibility to type 2 diabetes mellitus," *Nature Genetics*, vol. 40, no. 9, pp. 1092–1097, 2008.

[12] R. Saxena, B. F. Voight, V. Lyssenko et al., "Genome-wide association analysis identifies loci for type 2 diabetes and triglyceride levels," *Science*, vol. 316, no. 5829, pp. 1331–1336, 2007.

[13] L. J. Scott, K. L. Mohlke, L. L. Bonnycastle et al., "A genome-wide association study of type 2 diabetes in Finns detects multiple susceptibility variants," *Science*, vol. 316, no. 5829, pp. 1341–1345, 2007.

[14] R. Sladek, G. Rocheleau, J. Rung et al., "A genome-wide association study identifies novel risk loci for type 2 diabetes," *Nature*, vol. 445, no. 7130, pp. 881–885, 2007.

[15] V. Steinthorsdottir, G. Thorleifsson, I. Reynisdottir et al., "A variant in CDKAL1 influences insulin response and risk of type 2 diabetes," *Nature Genetics*, vol. 39, no. 6, pp. 770–775, 2007.

[16] E. Zeggini, M. N. Weedon, C. M. Lindgren et al., "Replication of genome-wide association signals in UK samples reveals risk loci for type 2 diabetes," *Science*, vol. 316, no. 5829, pp. 1336–1341, 2007.

[17] I. Prokopenko, M. I. McCarthy, and C. M. Lindgren, "Type 2 diabetes: new genes, new understanding," *Trends in Genetics*, vol. 24, no. 12, pp. 613–621, 2008.

[18] E. Zeggini, L. J. Scott, R. Saxena et al., "Meta-analysis of genome-wide association data and large-scale replication identifies additional susceptibility loci for type 2 diabetes," *Nature Genetics*, vol. 40, no. 5, pp. 638–645, 2008.

[19] J. R. Lupski, "Genomic rearrangements and sporadic disease," *Nature Genetics*, vol. 39, no. 7s, pp. S43–S47, 2007.

[20] D. F. Conrad, D. Pinto, R. Redon et al., "Origins and functional impact of copy number variation in the human genome," *Nature*, vol. 464, no. 7289, pp. 704–712, 2010.

[21] H. Park, J. I. Kim, Y. S. Ju et al., "Discovery of common Asian copy number variants using integrated high-resolution array CGH and massively parallel DNA sequencing," *Nature Genetics*, vol. 42, no. 5, pp. 400–405, 2010.

[22] A. J. Sharp, D. P. Locke, S. D. McGrath et al., "Segmental duplications and copy-number variation in the human genome," *American Journal of Human Genetics*, vol. 77, no. 1, pp. 78–88, 2005.

[23] G. M. Cooper, T. Zerr, J. M. Kidd, E. E. Eichler, and D. A. Nickerson, "Systematic assessment of copy number variant detection via genome-wide SNP genotyping," *Nature Genetics*, vol. 40, no. 10, pp. 1199–1203, 2008.

[24] R. Redon, S. Ishikawa, K. R. Fitch et al., "Global variation in copy number in the human genome," *Nature*, vol. 444, no. 7118, pp. 444–454, 2006.

[25] Y. Seino, K. Nanjo, N. Tajima et al., "Report of the committee on the classification and diagnostic criteria of diabetes mellitus," *Journal of the Japan Diabetes Society*, vol. 53, no. 6, pp. 450–467, 2010.

[26] H. Stefansson, D. Rujescu, S. Cichon et al., "Large recurrent microdeletions associated with schizophrenia," *Nature*, vol. 455, no. 7210, pp. 232–236, 2008.

[27] M. T. Barrett, A. Scheffer, A. Ben-Dor et al., "Comparative genomic hybridization using oligonucleotide microarrays and total genomic DNA," *Proceedings of the National Academy of Sciences of the United States of America*, vol. 101, no. 51, pp. 17765–17770, 2004.

[28] G. H. Perry, A. Ben-Dor, A. Tsalenko et al., "The fine-scale and complex architecture of human copy-number variation," *American Journal of Human Genetics*, vol. 82, no. 3, pp. 685–695, 2008.

[29] A. J. de Smith, A. Tsalenko, N. Sampas et al., "Array CGH analysis of copy number variation identifies 1284 new genes variant in healthy white males: implications for association studies of complex diseases," *Human Molecular Genetics*, vol. 16, no. 23, pp. 2783–2794, 2007.

[30] A. J. Sharp, S. Hansen, R. R. Selzer et al., "Discovery of previously unidentified genomic disorders from the duplication architecture of the human genome," *Nature Genetics*, vol. 38, no. 9, pp. 1038–1042, 2006.

[31] J. R. Lupski, "Genomic disorders ten years on," *Genome Medicine*, vol. 1, no. 4, p. 42, 2009.

[32] I. Ionita-Laza, A. J. Rogers, C. Lange, B. A. Raby, and C. Lee, "Genetic association analysis of copy-number variation (CNV) in human disease pathogenesis," *Genomics*, vol. 93, no. 1, pp. 22–26, 2009.

[33] C. Shtir, R. Pique-Regi, K. Siegmund, J. Morrison, F. Schumacher, and P. Marjoram, "Copy number variation in the Framingham Heart Study," *BioMed Central Proceedings*, vol. 3, supplement 7, p. S133, 2009.

[34] The Wellcome Trust Case Control Consortium, "Genome-wide association study of CNVs in 16,000 cases of eight common diseases and 3,000 shared controls," *Nature*, vol. 464, no. 7289, pp. 713–720, 2010.

[35] International Human Genome Sequencing Consortium, "Finishing the euchromatic sequence of the human genome," *Nature*, vol. 431, no. 7011, pp. 931–945, 2004.

[36] E. E. Eichler, J. Flint, G. Gibson et al., "Missing heritability and strategies for finding the underlying causes of complex disease," *Nature Reviews Genetics*, vol. 11, no. 6, pp. 446–450, 2010.

[37] C. M. Lese, J. A. Fantes, H. C. Riethman, and D. H. Ledbetter, "Characterization of physical gap sizes at human telomeres," *Genome Research*, vol. 9, no. 9, pp. 888–894, 1999.

[38] E. E. Eichler, R. A. Clark, and X. She, "An assessment of the sequence gaps: unfinished business in a finished human genome," *Nature Reviews Genetics*, vol. 5, no. 5, pp. 345–354, 2004.

[39] K. Devriendt and J. R. Vermeesch, "Chromosomal phenotypes and submicroscopic abnormalities," *Human genomics*, vol. 1, no. 2, pp. 126–133, 2004.

[40] G. Van Buggenhout, C. Melotte, B. Dutta et al., "Mild Wolf-Hirschhorn syndrome: micro-array CGH analysis of atypical 4p16.3 deletions enables refinement of the genotype-phenotype map," *Journal of Medical Genetics*, vol. 41, no. 9, pp. 691–698, 2004.

[41] A. Itsara, G. M. Cooper, C. Baker et al., "Population analysis of large copy number variants and hotspots of human genetic disease," *American Journal of Human Genetics*, vol. 84, no. 2, pp. 148–161, 2009.

[42] D. A. Swartz, E. I. Park, W. J. Visek, and J. Kaput, "The e subunit gene of murine FF-ATP synthase. Genomic sequence, chromosomal mapping, and diet regulation," *Journal of Biological Chemistry*, vol. 271, no. 34, pp. 20942–20948, 1996.

[43] T. Hayakawa, M. Noda, K. Yasuda et al., "Ethidium bromide-induced inhibition of mitochondrial gene transcription suppresses glucose-stimulated insulin release in the mouse pancreatic beta-cell cell line betaHC9," *Journal of Biological Chemistry*, vol. 273, no. 32, pp. 20300–20307, 1998.

[44] A. Abderrahmani, G. Niederhauser, V. Plaisance et al., "Complexin I regulates glucose-induced secretion in pancreatic beta-cells," *Journal of Cell Science*, vol. 117, no. 11, pp. 2239–2247, 2004.

[45] M. Dubois, P. Vacher, B. Roger et al., "Glucotoxicity inhibits late steps of insulin exocytosis," *Endocrinology*, vol. 148, no. 4, pp. 1605–1614, 2007.

[46] Y. Kanaoka, S. H. Kimura, I. Okazaki, M. Ikeda, and H. Nojima, "GAK: a cyclin G associated kinase contains a tensin/auxilin-like domain," *Federation of European Biochemical Societies Letters*, vol. 402, no. 1, pp. 73–80, 1997.

[47] S. H. Kimura, H. Tsuruga, N. Yabuta, Y. Endo, and H. Nojima, "Structure, expression, and chromosomal localization of human GAK," *Genomics*, vol. 44, no. 2, pp. 179–187, 1997.

[48] F. Y. Wei, K. Nagashima, T. Ohshima et al., "Cdk5-dependent regulation of glucose-stimulated insulin secretion," *Nature Medicine*, vol. 11, no. 10, pp. 1104–1108, 2005.

[49] M. Ubeda, J. M. Rukstalis, and J. F. Habener, "Inhibition of cyclin-dependent kinase 5 activity protects pancreatic beta cells from glucotoxicity," *Journal of Biological Chemistry*, vol. 281, no. 39, pp. 28858–28864, 2006.

[50] K. Kitani, S. Oguma, T. Nishiki et al., "A Cdk5 inhibitor enhances the induction of insulin secretion by exendin-4 both in vitro and in vivo," *Journal of Physiological Sciences*, vol. 57, no. 4, pp. 235–239, 2007.

[51] A. H. Talukder, Q. Meng, and R. Kumar, "CRIPak, a novel endogenous Pak1 inhibitor," *Oncogene*, vol. 25, no. 9, pp. 1311–1319, 2006.

[52] Z. Wang, E. Oh, and D. C. Thurmond, "Glucose-stimulated Cdc42 signaling is essential for the second phase of insulin secretion," *Journal of Biological Chemistry*, vol. 282, no. 13, pp. 9536–9546, 2007.

[53] M. Wiedemann and B. Trueb, "Characterization of a novel protein (FGFRL1) from human cartilage related to FGF receptors," *Genomics*, vol. 69, no. 2, pp. 275–279, 2000.

[54] A. A. Hardikar, B. Marcus-Samuels, E. Geras-Raaka, B. M. Raaka, and M. C. Gershengorn, "Human pancreatic precursor cells secrete FGF2 to stimulate clustering into hormone-expressing islet-like cell aggregates," *Proceedings of the National Academy of Sciences of the United States of America*, vol. 100, no. 12, pp. 7117–7122, 2003.

[55] S. Arnaud-Dabernat, M. Kritzik, A. G. Kayali et al., "FGFR3 is a negative regulator of the expansion of pancreatic epithelial cells," *Diabetes*, vol. 56, no. 1, pp. 96–106, 2007.

[56] S. D. Gerber, F. Steinberg, M. Beyeler, P. M. Villiger, and B. Trueb, "The murine Fgfrl1 receptor is essential for the development of the metanephric kidney," *Developmental Biology*, vol. 335, no. 1, pp. 106–119, 2009.

[57] C. M. Sadek, S. Jalaguier, E. P. Feeney et al., "Isolation and characterization of AINT: a novel ARNT interacting protein expressed during murine embryonic development," *Mechanisms of Development*, vol. 97, no. 1-2, pp. 13–26, 2000.

[58] C. M. Sadek, M. Pelto-Huikko, M. Tujague, K. R. Steffensen, M. Wennerholm, and J. A. Gustafsson, "TACC3 expression is tightly regulated during early differentiation," *Gene Expression Patterns*, vol. 3, no. 2, pp. 203–211, 2003.

[59] J. Qiu, Y. H. Ni, R. H. Chen et al., "Gene expression profiles of adipose tissue of obese rats after central administration of neuropeptide Y-Y5 receptor antisense oligodeoxynucleotides by cDNA microarrays," *Peptides*, vol. 29, no. 11, pp. 2052–2060, 2008.

[60] C. Vernochet, S. B. Peres, K. E. Davis et al., "C/EBPalpha and the corepressors CtBP1 and CtBP2 regulate repression of select visceral white adipose genes during induction of the brown phenotype in white adipocytes by peroxisome proliferator-activated receptor gamma agonists," *Molecular and Cellular Biology*, vol. 29, no. 17, pp. 4714–4728, 2009.

[61] R. Simon, T. Lufkin, and A. D. Bergemann, "Homeobox gene Sax2 deficiency causes an imbalance in energy homeostasis," *Developmental Dynamics*, vol. 236, no. 10, pp. 2792–2799, 2007.

[62] T. Kato, M. Emi, H. Sato et al., "Segmental copy-number gain within the region of isopentenyl diphosphate isomerase genes in sporadic amyotrophic lateral sclerosis," *Biochemical and Biophysical Research Communications*, vol. 402, no. 2, pp. 438–442, 2010.

Supplemental Material can be found at:
http://www.jbc.org/content/suppl/2011/03/17/M110.206904.DC1.html

THE JOURNAL OF BIOLOGICAL CHEMISTRY VOL. 286, NO. 23, pp. 20812–20822, June 10, 2011
© 2011 by The American Society for Biochemistry and Molecular Biology, Inc. Printed in the U.S.A.

Peptidyl-prolyl Cis/Trans Isomerase NIMA-interacting 1 Associates with Insulin Receptor Substrate-1 and Enhances Insulin Actions and Adipogenesis[S]

Received for publication, November 29, 2010, and in revised form, February 16, 2011 Published, JBC Papers in Press, March 17, 2011, DOI 10.1074/jbc.M110.206904

Yusuke Nakatsu[‡1], Hideyuki Sakoda[§1], Akifumi Kushiyama[¶1], Jun Zhang[‡], Hiraku Ono[§], Midori Fujishiro[§], Takako Kikuchi[§], Toshiaki Fukushima[‡], Masayasu Yoneda[‡], Haruya Ohno[‡], Nanao Horike[‖], Machi Kanna[‡], Yoshihiro Tsuchiya[‡], Hideaki Kamata[‡], Fusanori Nishimura[**], Toshiaki Isobe[‡‡], Takehide Ogihara[§§], Hideki Katagiri[§§], Yoshitomo Oka[§§], Shin-ichiro Takahashi[¶¶], Hiroki Kurihara[‖], Takafumi Uchida[‖‖], and Tomoichiro Asano[‡2]

From the [‡]Department of Medical Science, Graduate School of Medicine, University of Hiroshima, 1-2-3 Kasumi, Minami-ku, Hiroshima City, Hiroshima 734-8553, Japan, the [§]Department of Internal Medicine, Graduate School of Medicine, University of Tokyo, 7-3-1 Hongo, Bunkyo-ku, Tokyo 113-0033, the [¶]Institute for Adult Disease, Asahi Life Foundation, Tokyo 100-0006, the [**]Department of Dental Science for Health Promotion, Hiroshima University Graduate School of Biomedical Sciences, Hiroshima 734-8553, the [‡‡]Center for Priority Areas, Tokyo Metropolitan University, Hachioji, Tokyo 192-0397, Japan, the [§§]Division of Molecular Metabolism and Diabetes, Tohoku University Graduate School of Medicine, 2-1 Seiryo-machi, Aoba-ku, Sendai 980-8575, Japan, the [‖]Department of Physiological Chemistry and Metabolism, Graduate School of Medicine, University of Tokyo, 7-3-1 Hongo, Bunkyo-ku 113-0033, Tokyo, the [¶¶]Department of Applied Biological Chemistry, Graduate School of Agricultural and Life Sciences, The University of Tokyo, Bunkyo-ku, Tokyo, Japan, and the [‖‖]Department of Molecular Cell Biology, Graduate School of Agricultural Science, Tohoku University, Sendai, 113-0033 Miyagi, Japan

Peptidyl-prolyl cis/trans isomerase NIMA-interacting 1 (Pin1) is a unique enzyme that associates with the pSer/Thr-Pro motif and catalyzes cis-trans isomerization. We identified Pin1 in the immunoprecipitates of overexpressed IRS-1 with myc and FLAG tags in mouse livers and confirmed the association between IRS-1 and Pin1 by not only overexpression experiments but also endogenously in the mouse liver. The analysis using deletion- and point-mutated Pin1 and IRS-1 constructs revealed the WW domain located in the N terminus of Pin1 and Ser-434 in the SAIN (Shc and IRS-1 NPXY binding) domain of IRS-1 to be involved in their association. Subsequently, we investigated the role of Pin1 in IRS-1 mediation of insulin signaling. The overexpression of Pin1 in HepG2 cells markedly enhanced insulin-induced IRS-1 phosphorylation and its downstream events: phosphatidylinositol 3-kinase binding with IRS-1 and Akt phosphorylation. In contrast, the treatment of HepG2 cells with Pin1 siRNA or the Pin1 inhibitor Juglone suppressed these events. In good agreement with these *in vitro* data, Pin1 knock-out mice exhibited impaired insulin signaling with glucose intolerance, whereas adenoviral gene transfer of Pin1 into the *ob/ob* mouse liver mostly normalized insulin signaling and restored glucose tolerance. In addition, it was also demonstrated that Pin1 plays a critical role in adipose differentiation, making Pin1 knock-out mice resistant to diet-induced obesity. Importantly, Pin1 expression was shown to be up-regulated in accordance with nutrient conditions such as food intake or a high-fat diet. Taken together, these observations indicate that Pin1 binds to IRS-1 and thereby markedly enhances insulin action, essential for adipogenesis.

Peptidyl-prolyl cis/trans isomerases constitute a special class of enzymes that function not by modifying other peptides covalently but only by producing conformational changes (1–4). Pin1, one of the peptidyl-prolyl cis/trans isomerase isoforms that is distinct from the two major classes of isomerases, the cyclophilins and the FK506-binding proteins (5, 6), was initially cloned as a NIMA kinase interacting protein (7) and specifically recognizes a proline bond preceded by a phosphorylated serine or threonine residue (phospho-Ser/Thr-Pro motif) with a WW domain at its N terminus (8, 9). Then, its C-terminal PPIase domain was shown to catalyze cis-trans isomerization of the target peptidyl-prolyl bonds and thereby modify the actions of target proteins (8, 9). Since its discovery, numerous proteins have been identified as Pin1 substrates (8, 10), implicating it in the regulation of many biological processes. For example, Pin1 inhibits the phosphorylation of Cdc25 and controls the replication checkpoint in the cell cycle (11, 12). Pin1 also stabilizes the tumor suppressor p53 and is abundantly expressed in some malignant tumors, suggesting involvement in malignant transformation (13, 14). On the other hand, Pin1 is also expressed at high levels in most neurons (15, 16). Although much remains to be clarified regarding the role of Pin1 in neurons, it reportedly protects against neurodegeneration via several independent mechanisms (15, 16), as supported by the fact that Pin1 knock-out (KO) mice exhibit abnormal central nervous function (15, 16). In addition, the enzymatic function of Pin1 is reportedly inactivated by oxidative stress modification occurring in the early stages of Alzheimer disease, implicating Pin1 in brain function (16, 17). Therefore, Pin1 has been implicated in the pathogenesis of two major disorders; cancer and Alzheimer disease (9, 10).

Very recently, we reported that Pin1 expression is higher in the fed than in the fasted state and that Pin1 associates with CRTC2, a co-activator of CREB (cAMP-response element-binding protein), and suppresses CRE (cAMP-response ele-

[S] The on-line version of this article (available at http://www.jbc.org) contains supplemental Figs. 1–7.

[1] These authors contributed equally to this work.

[2] To whom correspondence should be addressed. Tel.: 81-82-257-5135; Fax: 81-82-257-5136; E-mail: asano-tky@umin.ac.jp.

Downloaded from www.jbc.org at TOHOKU UNIVERSITY, on April 18, 2012

ment) transcriptional activity (18). Suppressed CRE activity leads to reduced PEPCK expression and gluconeogenesis. In this study we newly identified Pin1 to be a positive regulator of insulin signaling via enhanced insulin-induced insulin receptor substrate-1 (IRS-1)[3] phosphorylation. In addition, Pin1 expression was revealed to be markedly increased by high-fat diet feeding. Because a high-fat diet is one of the most common causes of obesity, we also performed experiments to ascertain the effects of Pin1 on adipogenesis in this study. Herein, we present evidence that Pin1 plays a critical role in energy incorporation into the body by enhancing insulin signaling and adipogenesis. Our findings raise the possibility of Pin1 being a promising target molecule for treating diabetes mellitus.

EXPERIMENTAL PROCEDURES

Materials—Affinity-purified antibodies against IRS-1, IRS-2, phosphorylated tyrosine (4G10), and Akt/protein kinase B were prepared as previously described (19). Anti-Pin1 antibody was generated by immunizing rabbits with the peptide QMQKPFEDASFATRTGEMSGPVFTDSGIHIITRTE (amino acids 129–163 of human Pin1). Anti-FLAG tag antibody was purchased from Sigma, and antibodies against the p85 subunit of phosphatidylinositol 3-kinase, phospho-Ser-473 and phospho-Thr-308 of Akt, and anti-actin were from Cell Signaling Technology (Danvers, MA).

Cell Culture—Sf9 cells were grown in TC100 (Invitrogen) medium containing 10% fetal bovine serum (FBS) at 27 °C. HepG2 hepatoma cells and human preadipocyte were grown in Dulbecco's modified Eagle's medium (DMEM) containing 10% FBS at 37 °C in 5% (v/v) CO_2 in air. Mouse 3T3-L1 fibroblasts were maintained in DMEM containing 10% donor calf serum in an atmosphere of 10% CO_2 at 37 °C. Two days after the fibroblasts had reached confluence, differentiation was induced by treating the cells with DMEM containing 4 μg/ml dexamethasone, 200 nM insulin, 0.5 mmol/liter 3-isobutyl-1-methylxanthine, and 10% FBS for 48 h as described previously. Cells were fed DMEM supplemented with 10% FBS every other day and used as mature 3T3-L1 adipocytes at day 8 after the induction of differentiation.

Animals—Pin1 KO mice were generated as previously described (20), and $Pin1^{+/+}$ and $Pin1^{-/-}$ mice were obtained by breeding $Pin1^{+/-}$ mice. The genotype was determined by PCR and $Pin1^{+/-}$ mice were separated for breeding. Twelve-week-old $Pin1^{+/+}$ and $Pin1^{-/-}$ mice were fed a standard diet or high-fat diet (HFD) for 4 weeks. The nutrient composition of the standard diet was 54.4% carbohydrate, 23.6% protein, 5.3% fat with a vitamin and mineral mixture, whereas that of the HFD was 7.5% carbohydrate, 24.5% protein, 60% fat with a vitamin and mineral mixture. In other experiments, 12–16-week-old $Pin1^{+/+}$ and $Pin1^{-/-}$ mice were used.

Preparation of Adenoviruses Expressing MEF-tagged IRS Protein, Pin1, and GFP—The myc-TEV (tobacco etch virus)-FLAG (MEF) tag cassette was generated by DNA synthesis and inserted into cloning sites in the mammalian expression vector pcDNA3 (Invitrogen) and termed pcDNA3-MEF, as reported previously (19). To create the N-terminal MEF-tagged IRS-1 construct, human IRS-1 cDNA was inserted into pcDNA3-MEF. Then the coding portion of MEF-tagged IRS-1 was isolated from pcDNA3-MEF-IRS-1. Similarly, the coding regions of MEF-tagged IRS-2 and S434A IRS-1 were prepared. Recombinant adenovirus expressing MEF-tagged IRS-1, MEF-tagged S434A IRS-1, MEF-tagged IRS-2, human Pin1 with a C-terminal HA tag, GFP-tagged Pin1, and GFP were generated, and the adenovirus encoding *LacZ* served as a control. The recombinant adenoviruses expressing human Pin1 with a C-terminal HA tag and *LacZ* were used for adenoviral gene transfer into *ob*/*ob* mice.

Purification of MEF-tagged IRS-1-containing Complexes from Mouse Livers—Recombinant adenovirus expressing MEF-tagged IRS-1 was purified and concentrated using cesium chloride ultracentrifugation. Adenovirus encoding *LacZ* served as a control. Male C57B6 mice, 9 weeks of age, obtained from Nippon Bio-Supply Center (Tokyo, Japan), were injected via the tail vein with adenovirus at a dose of 2.5×10^7 plaque-forming units/g of body wt. Four days later, mouse livers were removed and lysed in lysis buffer (50 mM Tris-HCl, pH 7.5, 150 mM NaCl, 10% (w/v) glycerol, 100 mM NaF, 10 mM EGTA, 1 mM Na_3VO_4, 1% (w/v) Triton X-100, 5 μM $ZnCl_2$, 2 mM PMSF, 10 μg/ml aprotinin, and 1 μg/ml leupeptin). Lysates were centrifuged at 100,000 × *g* for 20 min at 4 °C. Supernatants were passed through a 5-μm filter, incubated with 150 μl of Sepharose beads for 60 min at 4 °C, and then passed through a 0.65-μm filter. The filtrated supernatant was mixed with 150 μl of anti-myc-conjugated Sepharose beads for the first immunoprecipitation. After incubation for 90 min at 4 °C, the beads were washed 5 times with 1.5 ml of TNTG buffer (20 mM Tris-HCl, pH 7.5, 150 mM NaCl, 10% (w/v) glycerol, and 0.1% (w/v) Triton X-100), twice with buffer A (20 mM Tris-HCl, pH 7.5, 150 mM NaCl, and 0.1% (w/v) Triton X-100), and finally once with TNT buffer (50 mM Tris-HCl, pH 8.0, 150 mM NaCl, and 0.1% (w/v) Triton X-100). The washed beads were incubated with 15 units of tobacco etch virus protease (Invitrogen) in 150 μl of TNT buffer to release bound materials from the beads. After incubation for 60 min at room temperature, supernatants were pooled, and the beads were washed twice with 75 μl of buffer A. The resulting supernatants were combined and incubated with 25 μl of FLAG-Sepharose beads for the second immunoprecipitation. After a 60-min incubation at room temperature, the beads were washed 3 times with 500 μl of buffer A, and proteins bound to the FLAG beads were dissociated by incubation with 1 mM synthetic FLAG peptides in buffer A for 120 min at 4 °C. Approximately 3 μg of protein (0.01% of starting materials) were routinely recovered by this procedure. The samples were electrophoresed and subjected to SDS-PAGE and immunoblotting.

Immunoprecipitation and Immunoblotting—The cells were solubilized with Laemmli buffer (0.2 M Tris-HCl, 4% SDS, 10% glycerol, 5% 2-mercaptoethanol, 0.1% bromphenol blue). Equal amounts of protein from whole cell lysates were resolved by SDS-PAGE. Then the proteins were transferred to polyvinylidene difluoride membranes (Millipore, Billerica, MA) using an electroblotting apparatus (Mighty Small

[3] The abbreviations used are: IRS-1, insulin receptor substrate-1; HFD, high-fat diet; SAIN, Shc and IRS-1 NPXY binding; PPAR, peroxisome proliferator-activated receptor; MEF, myc-TEV (tobacco etch virus)-Flag.

Downloaded from www.jbc.org at TOHOKU UNIVERSITY, on April 18, 2012

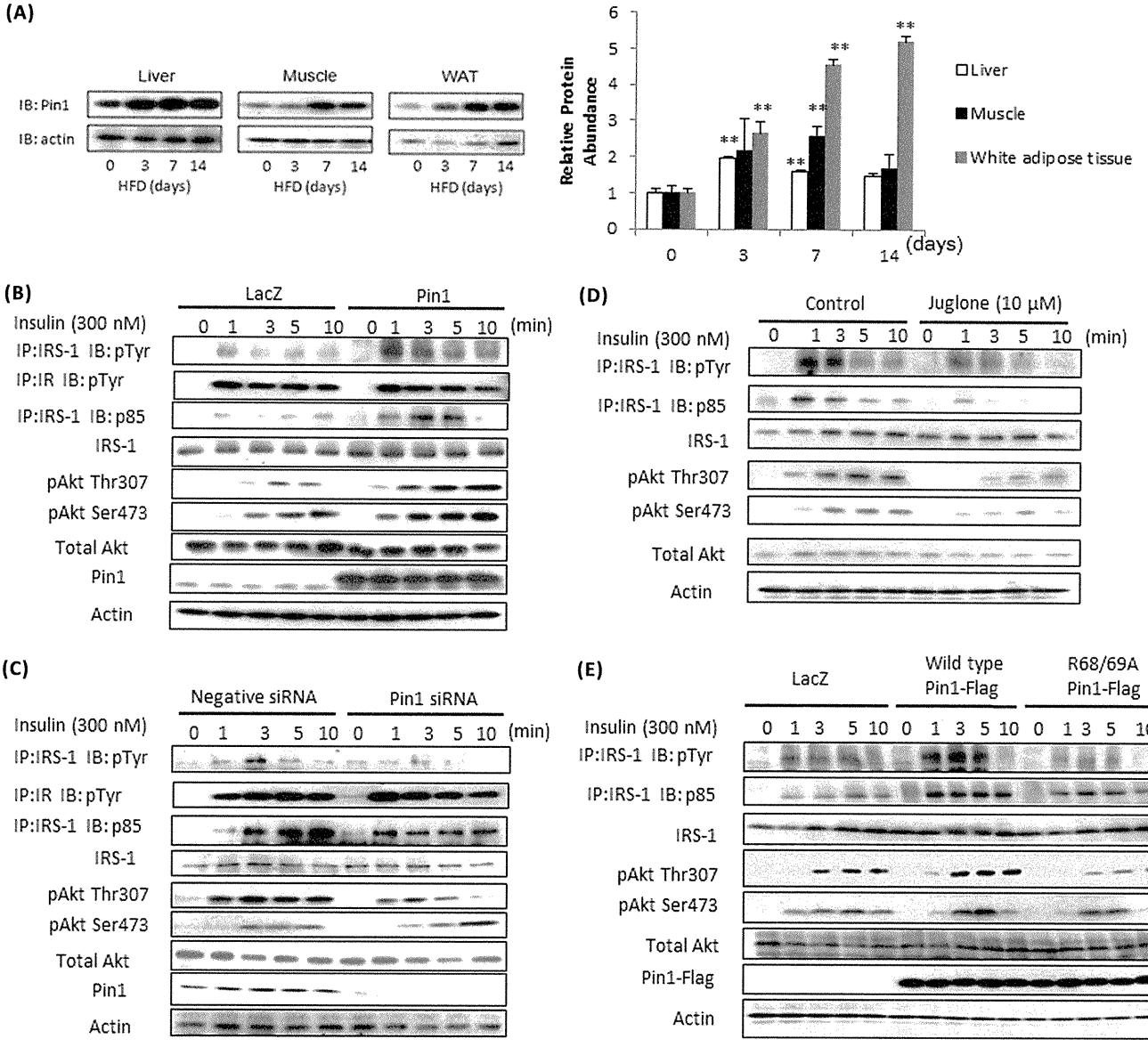

FIGURE 1. **Pin1 enhances insulin signaling.** *A*, mice were fed a control diet or HFD for the indicated periods. Liver, muscle, and adipose tissue lysates were prepared, then immunoblotted (*IB*) with anti-Pin1 or anti-actin antibody. *B* and *C*, Pin1 enhances insulin-induced IRS-1 phosphorylation and its downstream signaling. *B*, LacZ or Pin1 was overexpressed in HepG2 cells. *IP*, immunoprecipitates. *C*, HepG2 cells were treated with control siRNA or Pin1 siRNA. In both experiments, at the indicated times after initiating insulin stimulation, lysates were prepared from HepG2 cells. Then phosphorylation levels and protein amounts of IRS-1, p85 associated with IRS-1 and Akt Thr-307 and Ser-473 phosphorylations, and the Pin1 were determined. *D*, the Pin1 inhibitor Juglone attenuated the insulin-induced IRS-1 phosphorylation in HepG2 cells. HepG2 cells were treated with or without 10 μM Juglone for 30 min. At the indicated times after initiating insulin stimulation, lysates were prepared from HepG2 cells. Then phosphorylation levels and protein amounts of IRS-1, p85 associated with IRS-1, Akt Thr-307 and Ser-473 phosphorylations were determined. *E*, wild-type, but not the inactive mutant of Pin1, enhanced insulin-induced IRS-1 phosphorylation and its downstream signaling. LacZ, wild-type Pin1, or R68A/R69A-mutated Pin1 was overexpressed in HepG2 cells. At the indicated times after initiating insulin stimulation, lysates were prepared from HepG2 cells. Then, phosphorylation levels and protein amounts of IRS-1, p85 associated with IRS-1, and Akt Thr-307 and Ser-473 phosphorylations were determined. A representative immunoblot from four independent experiments is shown.

Transphor; Amersham Biosciences) and subjected to immunoblotting using the Super Signal West Pico Chemiluminescence System (Pierce). The results of several immunoblots were quantitatively analyzed using an LAS-3000 mini (FUJIFILM, Tokyo, Japan).

Supernatants containing equal amounts of protein (2 mg) were incubated with anti-IRS-1 and anti-IRS-2 antibodies (5 μg each) and then with 100 μl of protein A- and G-Sepharose. These immunoprecipitates and cell lysates were boiled in Laemmli sample buffer containing 100 mmol/liter dithiothreitol, electrophoresed, and immunoblotted with anti-IRS-1, anti-IRS-2, anti-p85 (phosphatidylinositol-3-kinase), anti-Pin1, phospho-Akt (Thr-308 and Ser-473), or 4G10 antibody. The bands were quantitatively analyzed using the LAS-3000 mini.

Preparation of Baculovirus-produced Recombinant Proteins—Full-length coding regions of human Pin1, GFP-tagged Pin1, IRS-1, and DsRed-tagged full-length and deletion mutants of IRS-1 were subcloned into pBacPAK9 transfer vector (Clontech, Mountain View, CA), and baculoviruses were prepared according to the manufacturer's instructions. For protein production, Sf9 cells were infected with these baculoviruses and grown for 48 h.

Downloaded from www.jbc.org at TOHOKU UNIVERSITY, on April 18, 2012

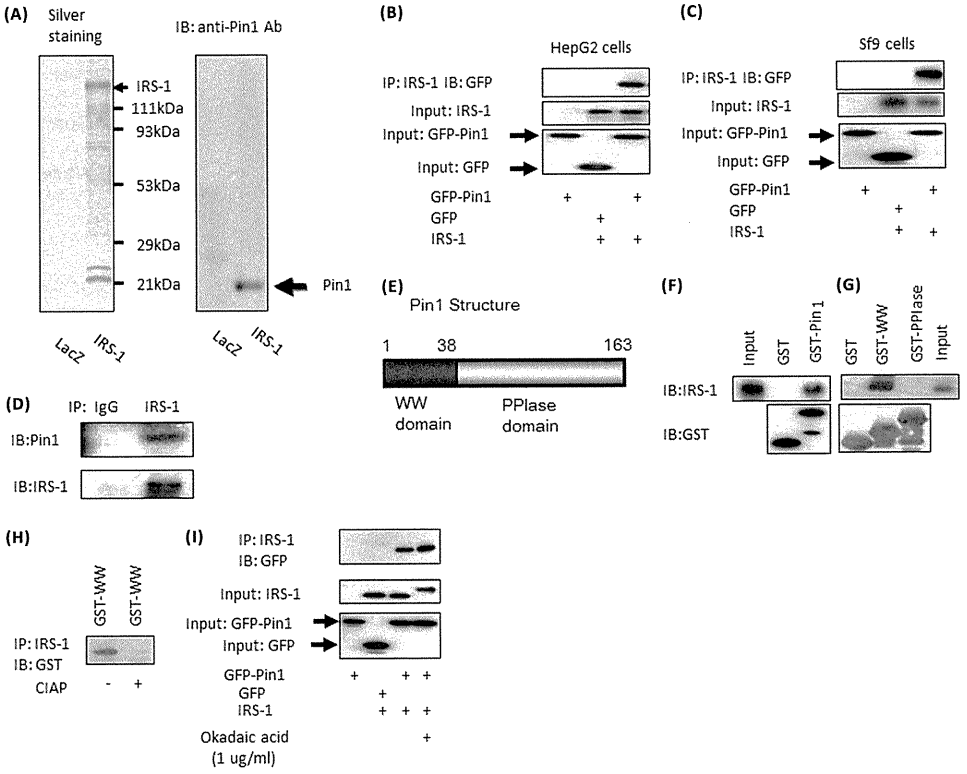

FIGURE 2. *A*, Pin1 association with IRS-1 is shown. IRS-1 with the N-terminal MEF tag was overexpressed in mouse liver using adenovirus gene transfer, and IRS-1-containing complexes were purified. The samples were electrophoresed, then silver-stained (*left panel*) and immunoblotted (*IB*) with anti-Pin1 antibody (*Ab*, *right panel*). *B*, IRS-1 or control LacZ was overexpressed with GFP or GFP-Pin1 in HepG2 cells. The cell lysates were immunoprecipitated (*IP*) with anti-IRS-1 antibody followed by immunoblotting with anti-GFP antibody. *C*, IRS-1 was overexpressed with GFP or GFP-Pin1 in Sf9 cells. The cell lysates were immunoprecipitated with anti-IRS-1 antibody followed by immunoblotting with anti-GFP antibody. *D*, the mouse liver cell lysates were immunoprecipitated with anti-IRS-1, and the immunoprecipitates were immunoblotted with anti-Pin1 and anti-IRS-1. *E*, Pin1 structure. GST-Pin1, GST-Pin1 WW domain, and GST-Pin1 PPIase domain were prepared. With incubation, these GST-proteins were conjugated to beads and cell lysates from IRS-1 overexpressing Sf-9 cells. *F*, GST-Pin1, but not GST alone, bound to IRS-1 *in vitro*. *G*, GST-WW, but not the GST-PPIase domain, bound IRS-1. *H*, lysates of Sf-9 cells overexprressing IRS-1 were treated with or without 40 units/ml alkaline phosphatase. Then the cell lysates were incubated with GST-WW domain and immunoprecipitated with anti-IRS-1 antibody. The immunoprecipitates were electrophoresed and immunoblotted with anti-GST antibody. *I*, HepG2 cells overexpressing IRS-1 or control LacZ were overexpressed with GFP or GFP-Pin1, then incubated with or without 1 μg/ml okadaic acid for 1 h. The cell lysates were immunoprecipitated with anti-IRS-1 antibody followed by immunoblotting with anti-GFP antibody.

Preparation of Glutathione S-transferase (GST)-Pin1 Fusion Protein—cDNAs encoding full-length human Pin1 and the WW and PPIase domains of Pin1 were subcloned into a pGEX-4T-1 vector (GE Healthcare), which was used to transform *Escherichia coli* JM105 (Promega, Madison, WI). Transformed cells were grown to an A_{600} of 0.6 in LB medium supplemented with 0.1 mg/ml ampicillin and stimulated for 3 h with 1.0 mM isopropyl-β-D-thiogalactopyranoside. GST fusion proteins were isolated and purified by affinity chromatography on a glutathione-Sepharose 4B column (GE Healthcare). Glutathione was removed by dialysis against phosphate-buffered saline containing 10 mM dithiothreitol.

RNA Interference—For the knockdown of human Pin1, a validated Stealth™ RNAi of human Pin1 (5′-CGGCAACAGCAGCAGUGGUGGCAAA-3′) was used. After RNAi and RNAiMAX in Opti-MEM had been mixed, they were introduced into HepG2. Forty-eight hours later, the cells were stimulated with insulin for the indicated times. Mouse Pin1 RNAi (5′-CACAGTATTTATTGTTCTAA-3′) was purchased from Invitrogen. Similarly, 48 h after introduction into 3T3-L1 cells, differentiation was induced by a mixture including isobutylmethylxanthine, dexamethasone, and insulin.

Intraperitoneal Glucose, Insulin, and Pyruvate Tolerance Tests—Mice were fasted for 14 h followed by blood sampling and intraperitoneal injection of glucose (2 g/kg body wt), insulin (0.75 units/kg body wt), or pyruvate (2 g/kg body wt). Whole venous blood was obtained from the tail vein at the indicated times after the glucose load. Blood glucose was measured with a portable blood glucose monitor.

In Vivo Insulin Stimulation—In brief, mice were anesthetized with pentobarbital sodium. The portal vein was exposed, and 0.4 ml of normal saline (0.9% NaCl) with or without insulin (25 milliunits/g of body wt) were injected. Livers were removed 30 s later, hind limb skeletal muscles 90 s thereafter, and immediately homogenized with a Polytron homogenizer in 6 volumes of solubilization buffer. Both extracts were centrifuged at 15,000 *g* for 30 min at 4 °C, and the supernatants were used as samples for immunoprecipitation and immunoblotting.

Glucose Uptake in Isolated Skeletal Muscle—Mice were anesthetized, and soleus muscles were dissected out and rapidly cut into 2–3-mg strips. Muscle strips were incubated in a shaking water bath at 35 °C for 60 min in a 20-ml flask containing 2.0 ml Krebs-Henseleit bicarbonate buffer supplemented with 8 mM glucose, 32 mM mannitol, and 0.1% bovine serum albumin

Downloaded from www.jbc.org at TOHOKU UNIVERSITY, on April 18, 2012

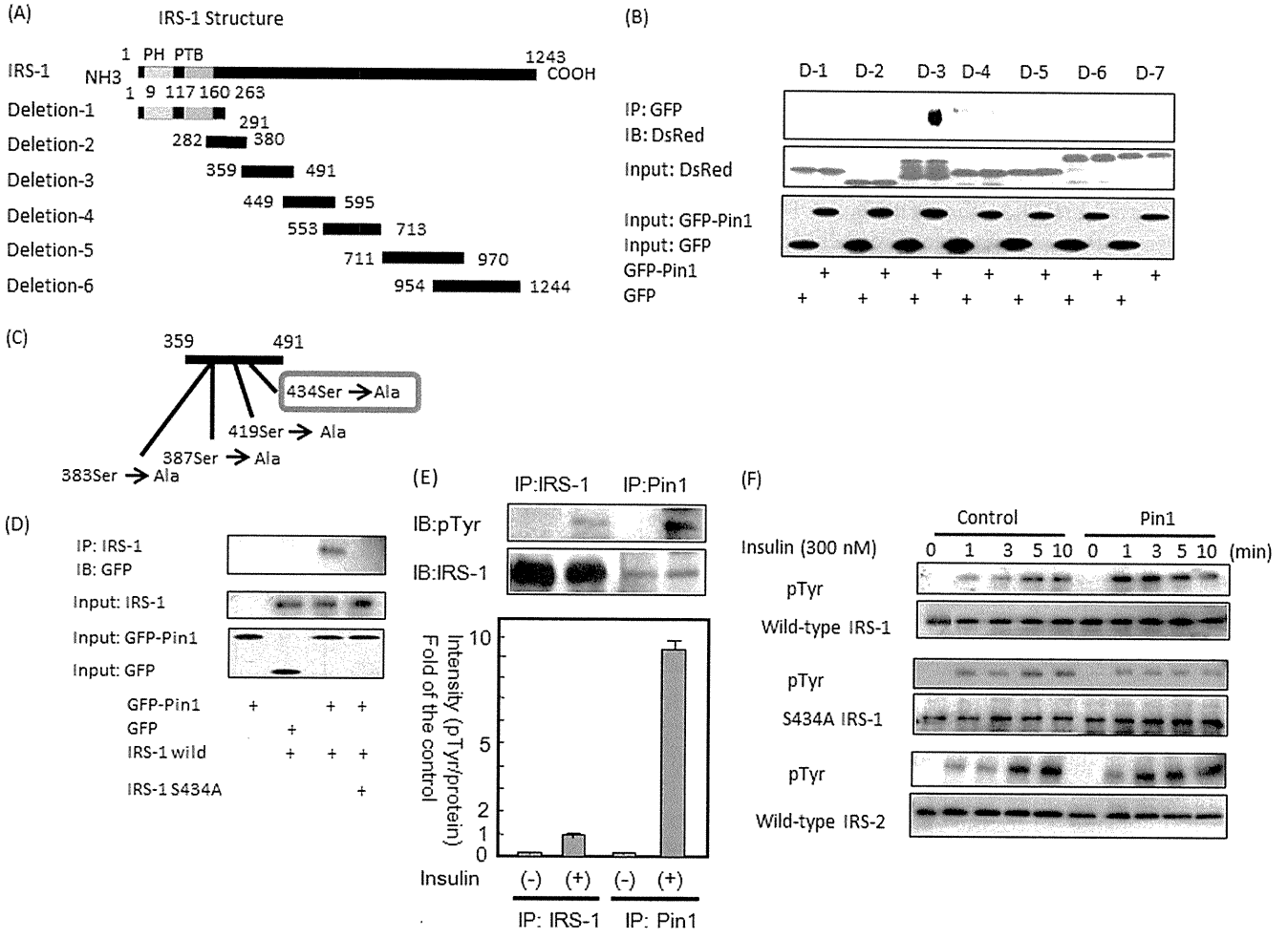

FIGURE 3. *A* and *B*, the constructs of IRS-1 deletion mutants are shown. Baculoviruses expressing these six mutants with the N-terminal DsRed tag were prepared. These six deletion mutants were overexpressed with GFP or GFP-Pin1 in Sf-9 cells. The cell lysates were immunoprecipitated (*IP*) with anti-GFP antibody followed by immunoblotting (*IB*) with anti-DsRed antibody. The *upper immunoblot* shows that mutant 3 binds to GFP-Pin1, but not to GFP alone. PH, pleckstrin homology; *PTB*, phosphotyrosine binding. *C* and *D*, shown are the orientations of four candidate Ser/Pro motifs in mutant 3 involved in the association with Pin1. Wild-type IRS-1 or IRS-1 S434A was overexpressed with GFP-Pin1 or GFP in Sf-9 cells. The cell lysates were immunoprecipitated with anti-IRS-1 antibody followed by immunoblotting with anti-GFP. The *upper panel* shows that, unlike the wild type, IRS-1 S434A does not associate with Pin1. *E*, HepG2 cells were stimulated with insulin for 3 min, then cell lysates were immunoprecipitated with anti-IRS-1 or anti-Pin1 antibody. Both samples were electrophoresed and immunoblotted with anti-Tyr(P) (*pTyr*) or anti-IRS-1 antibody (*upper panel*). The IRS-1 phosphorylation level and protein amount were calculated as the means ± S.E. of three samples (*, $p < 0.05$). *F*, MEF-tagged IRS-1, MEF-tagged S434A IRS-1, and MEF-tagged IRS-2 were overexpressed with control LacZ or Pin1 in HepG2 cells. Cell lysates were then immunoprecipitated with anti-FLAG-tag antibody and immunoblotted with anti-Tyr(P) and anti-FLAG-tag antibodies.

(BSA) (radioimmunoassay grade). Flasks were gassed continuously with 95% O_2, 5%CO_2 throughout the experiment. The muscles were then incubated for 20 min in oxygenated KRB buffer in the presence or absence of human insulin (2 milliunits/ml) and then incubated for 20 min at 29 °C in 1.5 ml of KRB buffer containing 8 mM 2-deoxy-D- [1,2-^{3}H(*N*)]glucose (2.25 μCi/ml), 32 mM [^{14}C]mannitol (0.3 μCi/ml), 2 mM sodium pyruvate, and 0.1% BSA. After the incubation, muscles were rapidly blotted, weighed, and solubilized with 1 ml of Soluene 350 (PerkinElmer Life Sciences). The samples were counted in a liquid scintillation counter. 2-Deoxy-[^{3}H]glucose uptake rates were corrected for extracellular trapping using [^{14}C]mannitol counts.

Quantitative Real-time Reverse Transcription-PCR—Total RNA was extracted from 3T3-L1 adipocytes or mouse liver and epididymal adipose tissue using Sepasol reagent (Nakalai Tesche, Kyoto, Japan). First-strand cDNAs were synthesized using PrimeScript reverse transcriptase with oligo(dT). Real-time PCR was performed using SYBR Green PCR master mix (Invitrogen) on an ABI Prism 7000 sequence detection system (Applied Biosystems, Foster City, CA). The primers were designed as follows: SREBP1 forward: GGAGCCATGGATTGCACATT; SREBP1 reverse, GGCCCGGGAAGTCACTGT; SREBP2 forward, TAACCCCTTGACTTCCTTGCT; SREBP2 reverse, TGCTCTTAGCCTCATCCTCAA; ACC forward, TCTCTGGCTTACAGGATGGTTTG; ACC reverse, GAGTCTATTTTCTTTCTGTCTCGACCTT; FAS forward, GCTGCGGAAACTTCAGGAAAT; FAS reverse, AGAGACGTGTCACTCCTGGACTT; SCD forward, GTCAAAGAGAAGGGCGGAAAAC; SCD reverse, AAGGTGTGGTGGTAGTTGTGGAAG.

Statistical Analysis—Results are expressed as the means ± S.E., and significance was assessed using one way analysis of variance unless otherwise indicated.

Downloaded from www.jbc.org at TOHOKU UNIVERSITY, on April 18, 2012

RESULTS

Increased Pin1 Expression in Mouse Liver, Muscle, and Fat Tissue with High-fat Diet Feeding—We previously reported that Pin1 protein is increased in the fed state (19). In this study we speculated that Pin1 expression might be regulated by altered nutrient conditions and examined Pin1 expression alteration in mice fed a HFD. As shown in Fig. 1*A*, HFD feeding markedly increased Pin1 protein in liver, muscle, and epididymal fat tissue. Pin1 amounts in other tissues such as the brain were not significantly altered (supplemental Fig. 1).

Enhancing Effect of Pin1 on Insulin Signaling—Because Pin1 expression was affected by nutrient conditions, we examined the possible involvement of Pin1 in glucose and lipid metabolism regulation. First, to elucidate the effect of Pin1 on insulin signaling, HA-tagged Pin1 was overexpressed in HepG2 cells (Fig. 1*B* and supplemental Fig. 2*A*). The overexpressed Pin1 amount was ~5-fold that of endogenous Pin1. In this state, insulin-induced IRS-1 phosphorylation and p85 association with IRS-1 and Akt phosphorylation were all markedly enhanced, whereas IRS-1 and Akt protein amounts were unchanged. Pin1 gene suppression using siRNA attenuated these events (Fig. 1*C* and supplemental Fig. 2*B*). Similar data were obtained using the Pin1-specific inhibitor Juglone, which has no effects on the activities of other prolyl isomerases, such as FKBP (FK506-binding protein) and cyclophilin A (21) (Fig. 1*D* and supplemental Fig. 2*C*). In addition, overexpression of the inactive mutant of Pin1 (R68A/R69A), in which Arg-68 and Arg-69 are replaced by Ala, failed to enhance insulin signaling (Fig. 1*E* and supplemental Fig. 2*D*). Thus, Pin1 expression level and activity regulate the efficiency of insulin-induced IRS-1 phosphorylation.

Association of Pin1 with IRS-1—Because Pin1 markedly enhanced insulin-induced IRS-1 phosphorylation, we considered a direct association of Pin1 with IRS-1. First, we used an MEF-tagged purification system, *i.e.* IRS-1 fused with N-terminal triple tags consisting of an myc tag, tobacco etch virus protease cleavage sequence, and FLAG tag overexpressed in mouse liver. Sequential affinity purification was performed using three steps; myc tag antibody immunoprecipitation, elution by tobacco etch virus protease digestion, and finally, FLAG tag antibody immunoprecipitation. Purified IRS-1 containing complexes were electrophoresed and then silver-stained, which demonstrated bait proteins of IRS-1 and many others including 14-3-3 proteins. Immunoblotting using Pin1 antibody indicated the presence of Pin1 in IRS-1 complexes (Fig. 2*A*). To confirm the association between IRS-1 and Pin1, IRS-1 and either GFP-Pin1 or GFP was co-overexpressed in HepG2 or Sf-9 cells. As shown in Fig. 2, *B* and *C*, GFP-Pin1, but not GFP alone, was detected in IRS-1 immunoprecipitates. Furthermore, Pin1 was detected in immunoprecipitates with anti-IRS-1 antibody, but not control IgG, from mouse liver (Fig. 2*D*). Thus, the association between IRS-1 and Pin1 is physiological.

To identify the Pin1 domain responsible for the association with IRS-1, GST-Pin1, the GST-Pin1 WW domain, and the GST-Pin1 PPIase domain were prepared (Fig. 2*E*). These GST proteins were conjugated to beads and incubated with cell lysates from IRS-1-overexpressing Sf-9 cells. GST-Pin1, but not

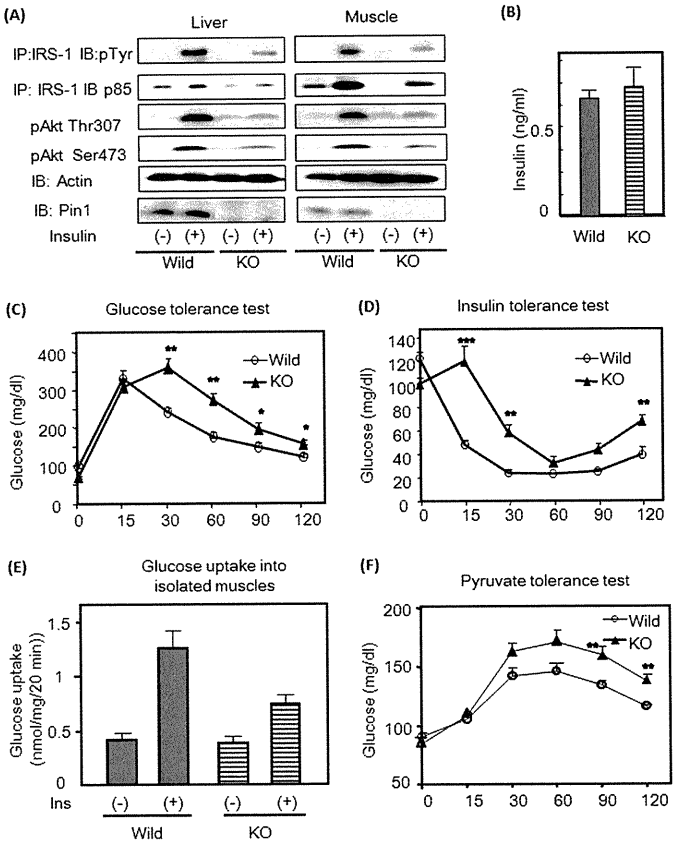

FIGURE 4. **Pin1 KO mice exhibit insulin resistance.** *A*, insulin was injected into control and Pin1 KO mice, and IRS-1 and Akt phosphorylations were determined. *IB*, immunoblot. *B*, fasting insulin concentrations in control and Pin1 KO mice are shown. *C*, glucose tolerance test results are shown. 2 mg/kg glucose was injected into control and Pin1 KO mice, and blood glucose concentrations were measured as indicated. *D*, insulin tolerance test results are shown. 0.75 units/kg insulin was injected intraperitoneally into control, and Pin1 KO mice and blood glucose concentrations were measured as indicated. *E*, shown is glucose uptake into isolated muscle. *F*, pyruvate tolerance test results are shown. 2 mg/kg pyruvate was injected into control, and Pin1 KO mice and blood glucose concentrations were measured, as indicated. The results are presented as the means (±S.E.) of six independent experiments (*, $p < 0.05$; **, $p < 0.01$).

GST alone, bound to IRS-1 *in vitro* (Fig. 2*F*). This pulldown system experiment revealed the GST-WW domain, but not that of GST-PPIase, to bind IRS-1 (Fig. 2*G*). In addition, treating IRS-1 with alkaline phosphatase completely abolished the association with Pin1 (Fig. 2*H*), whereas okadaic acid treatment significantly increased this association (Fig. 2*I*), suggesting involvement of serine and/or threonine phosphorylation in IRS-1.

Subsequently, six DsRed-tagged IRS-1 deletion (N termini) mutants (Fig. 3*A*) and GFP-tagged Pin1 were co-overexpressed in Sf-9 cells. As shown in Fig. 3*B*, the IRS-1 deletion mutant 3 containing amino acids 359–491 was immunoprecipitated with GFP-tagged Pin1. There are four serine-proline motifs in this portion (Fig. 3*C*). Each of these serine residues was replaced with alanine, and the mutant not associating with Pin1 was examined. As shown in Fig. 3*D*, IRS-1 with serine 434 replaced by alanine did not bind Pin1, indicating that the association between IRS-1 and Pin1 is mediated via the phosphoserine 434-containing motif in IRS-1 and the WW domain in Pin1. Ser-434 is in the SAIN (Shc and IRS-1 NPXY binding) domain, which

Downloaded from www.jbc.org at TOHOKU UNIVERSITY, on April 18, 2012

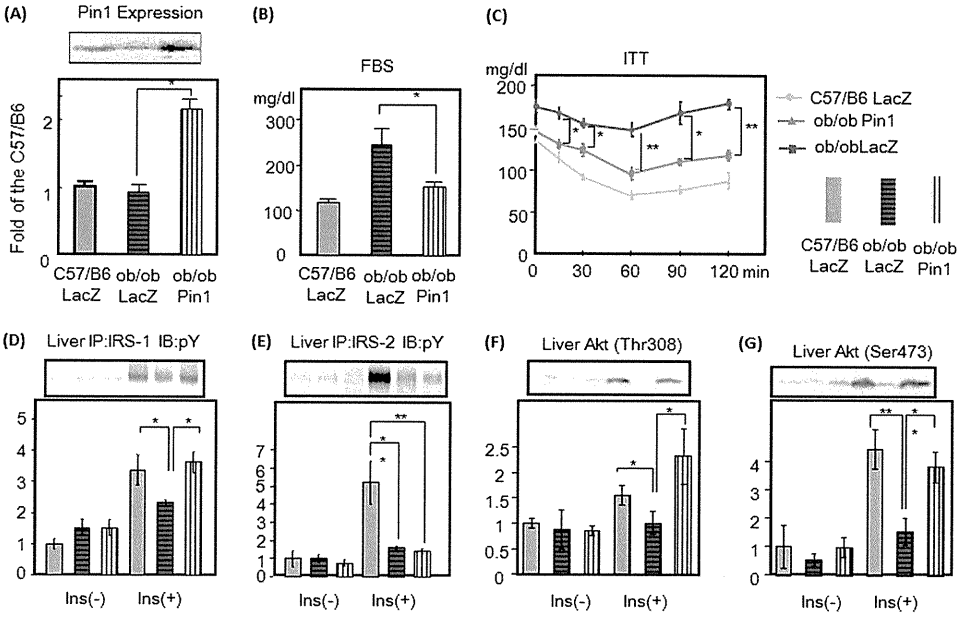

FIGURE 5. **Hepatic overexpression of Pin1 normalizes the hyperglycemia with insulin resistance in *ob/ob* mice.** LacZ or Pin1 adenovirus was injected via the tail vein. *A*, after 72 h, liver cell lysates were prepared, and the Pin1 expression level was determined by immunoblotting with anti-Pin1 antibody. The *upper panel* is a representative blot, and the *lower graph* shows the quantitative analysis ($n = 6$). *B*, shown are fasting blood glucose concentrations in C57/B6, *ob/ob* overexpressing LacZ, and *ob/ob* overexpressing Pin1 mice. *C*, insulin tolerance tests (*ITT*) for the three groups are shown. *D* and *E*, tyrosine phosphorylations of hepatic IRS-1 and IRS-2 are shown. Mice were injected with insulin via the portal vein, and phosphorylations of IRS-1 and IRS-2 were examined as reported previously. *IP*, immunoprecipitation; *pY*, Tyr(P). *F* and *G*, Akt phosphorylations at Thr-308 and Ser-473 were also examined in the livers of all three groups. $n = 6$ for each group and representative blots are shown in the *upper panels*. The results are presented as graphs with means (±S.E.). *, $p < 0.05$; **, $p < 0.05$.

has been suggested to be involved in the association with the activated insulin receptor (22, 23). IRS-1 contains many serine/threonine residues that are heavily phosphorylated even under basal conditions, and Ser-434 is probably one such residue.

Furthermore, to test whether or not enhanced IRS-1 phosphorylation is really mediated by direct association between IRS-1 and Pin1, insulin-induced phosphorylation levels of IRS-1 were compared between immunoprecipitation with IRS-1 antibody *versus* anti-Pin1 antibody using HepG2 cells. There was much less IRS-1 in the anti-Pin1 antibody immunoprecipitate than in the anti-IRS-1 immunoprecipitate, whereas insulin-induced IRS-1 phosphorylation was far greater with anti-Pin1 antibody immunoprecipitated IRS-1 (Fig. 3*E*). The tyrosine phosphorylation level/IRS-1 protein ratio was extremely high in the anti-Pin1 antibody immunoprecipitate as compared with the whole IRS-1 ratio. In addition, the effects of Pin1 on insulin-induced phosphorylations of S434A-mutated IRS-1 unable to associate with Pin1 as well as on IRS-2 were examined (Fig. 3*F*). FLAG-tagged wild-type, S434A IRS-1, or FLAG-tagged IRS-2 were co-overexpressed with Pin1 or LacZ in the HepG2 cells. The insulin-induced tyrosine phosphorylation of S434A IRS-1 was unaffected by Pin1 overexpression, whereas that of wild-type IRS-1 was markedly enhanced (Fig. 3*F*). It is noteworthy that IRS-2 phosphorylation is not significantly altered by Pin1. The phosphorylation of endogenous IRS-2 was also unaffected by Pin1 overexpression, although IRS-2 binds to Pin1 when overexpressed in HepG2 cells (supplemental Fig. 3). Our observations suggest that association of Pin1 with IRS-1 markedly enhances insulin-induced IRS-1 phosphorylation and its downstream signaling.

Insulin Resistance and Glucose Intolerance in Pin1 KO Mice—To elucidate the *in vivo* role of Pin1 in metabolism, the insulin signaling and sensitivity of Pin1 KO mice (20) were investigated. Insulin signaling was investigated first. Injecting insulin via the portal vein revealed insulin-induced IRS-1 tyrosine phosphorylation, the association of p85 with IRS-1 and Akt phosphorylation weaker in Pin1 KO liver and muscle than in those of wild-type mice (Fig. 4*A* and supplemental Fig. 4). Glucose and insulin tolerance tests demonstrated the insulin resistance of Pin1 KO mice (Fig. 4, *C* and *D*), whereas fasting serum insulin concentrations did not differ (Fig. 4*B*). The insulin-induced glucose uptake into isolated soleus muscle was also decreased in Pin1 KO mice as compared with controls, indicating muscle insulin resistance (Fig. 4*E*). The pyruvate tolerance test showed higher blood glucose concentrations in Pin1 KO mice, suggesting hepatic insulin resistance in these mice (Fig. 4*F*). Thus, in Pin1 KO mice, IRS-1 phosphorylation and downstream events are attenuated, and insulin resistance is present in both liver and muscle.

Hepatic Pin1 Overexpression Improves Insulin Resistance in ob/ob Mice—Interestingly, Pin1 expression was not altered in *ob/ob* mice as compared with lean controls. The reason is unclear, but we speculate that lack of a Pin1 expression response would exacerbate lipid and glucose metabolism abnormalities in *ob/ob* mice. We examined whether Pin1 overexpression might improve insulin resistance in *ob/ob* mice. Adenovirus for expressing Pin1 was injected intravenously. Adenovirus-mediated gene expression is reportedly limited to the liver (24) if adenovirus is injected into the bloodstream. Indeed, 72 h after injection, the amount of Pin1 was increased in the liver but not in muscle or adipose tissue (Fig. 5*A* and supplemental Fig. 5). In *ob/ob* mice, insulin-induced tyrosine phosphorylations of IRS-1 and IRS-2 and phosphatidylinositol 3-kinase/Akt activations were markedly impaired as

Downloaded from www.jbc.org at TOHOKU UNIVERSITY, on April 18, 2012

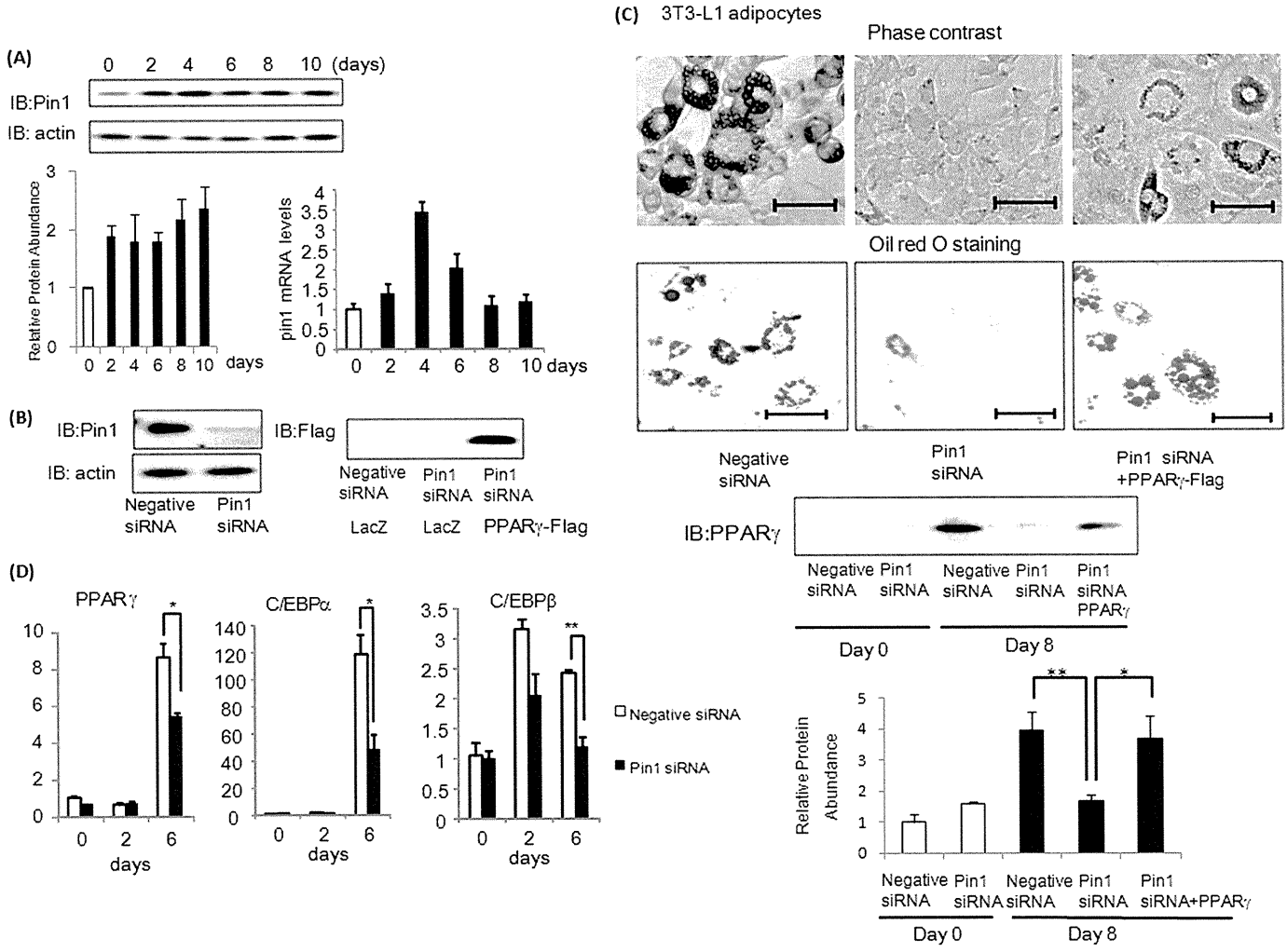

FIGURE 6. **Pin1 plays a critical role in adipose differentiation.** *A*, 3T3-L1 preadipocytes were induced to differentiate into adipocytes, and Pin1 protein and mRNA levels were determined at the indicated periods after initiation of differentiation. *IB*, immunoblots. *B*, 3T3-L1 preadipocytes were treated with Pin1 siRNA. The amounts of Pin1 and actin protein were determined with immunoblotting. *C*, 3T3-L1 preadipocytes were treated with control or Pin1 siRNA,or in combination with Pin1 siRNA and FLAG-tagged PPARγ adenovirus gene transfer. These cells were then induced to differentiate into adipocytes. Microscopic observations and oil red O staining results at 8 days are shown. Expression of PPARγ protein was detected as a marker of adipocyte maturity. *Scale bars* = 50 μm. *D*, before and 2 or 6 days after the induction of differentiation, PPARγ, c/EBPα, and c/EBPβ mRNA levels of 3T3-L1 cells were determined by real-time PCR. *, $p < 0.05$; **, $p < 0.05$.

reported previously (25) (Fig. 5, *D–G*). Pin1 overexpression normalized the decreased insulin-induced IRS-1, but not IRS-2, phosphorylation (Fig. 5, *D* and *E*). Hepatic Akt phosphorylations were also restored by Pin1 overexpression (Fig. 5, *F* and *G*). As reflected by improved insulin-signaling, glucose tolerance improved, *i.e.* fasting glucose concentrations (Fig. 5*B*) and expression levels of PEPCK and glucose-6-phosphatase were normalized (supplemental Fig. 6). The insulin tolerance test response was also improved (Fig. 5*C*). Thus, Pin1 overexpression improves insulin sensitivity in *ob/ob* mice.

Critical Role of Pin1 in Adipose Differentiation—Given the known role of insulin in adipose differentiation (26) and the increased Pin1 expression in WAT with HFD feeding, we speculated that Pin1 plays a critical role in diet-induced adipogenesis. First, Pin1 expression was shown to be up-regulated in 3T3-L1 cells during adipose differentiation (Fig. 6*A*). Then, the effect of Pin1 gene silencing using siRNA on adipose differentiation of 3T3-L1 adipocytes or human preadipocytes was examined (Fig. 6, *B* and *C*, and supplemental Fig. 7). Adipose differentiation of these cells was markedly impaired with suppressed inductions of PPARγ, c/EBPα, and C/EBPβ, known as master regulator genes of adipose differentiation (27–29) (Fig. 6*D*). In addition, expression of PPARγ protein, a marker of mature adipocytes, was reduced by Pin1 knockdown (Fig. 6*C*). Compensatory overexpression of PPARγ overcomes the suppressive effect of Pin1 siRNA on adipose differentiation (Fig. 6*C*).

Next, the adipose tissue of Pin1 KO mice was investigated. In normal mouse epididymal adipose tissue, PPARγ, c/EBPα, and CEBP/β as well as SREBP1, SREBP2, acetyl-CoA carboxylase, fatty acid synthase, and stearoyl-CoA-desaturase were markedly up-regulated by HFD feeding, which contributed to the enlargement of adipose tissues. In contrast, in Pin1 KO mouse adipose tissues, these increased gene expressions were significantly suppressed (Fig. 7, *A* and *B*), thereby markedly suppressing adipose tissue enlargement and weight gain on the HFD (Fig. 7, *C* and *D*). Thus, we concluded that Pin1 is a key regulator of diet-induced adipo-

Downloaded from www.jbc.org at TOHOKU UNIVERSITY, on April 18, 2012

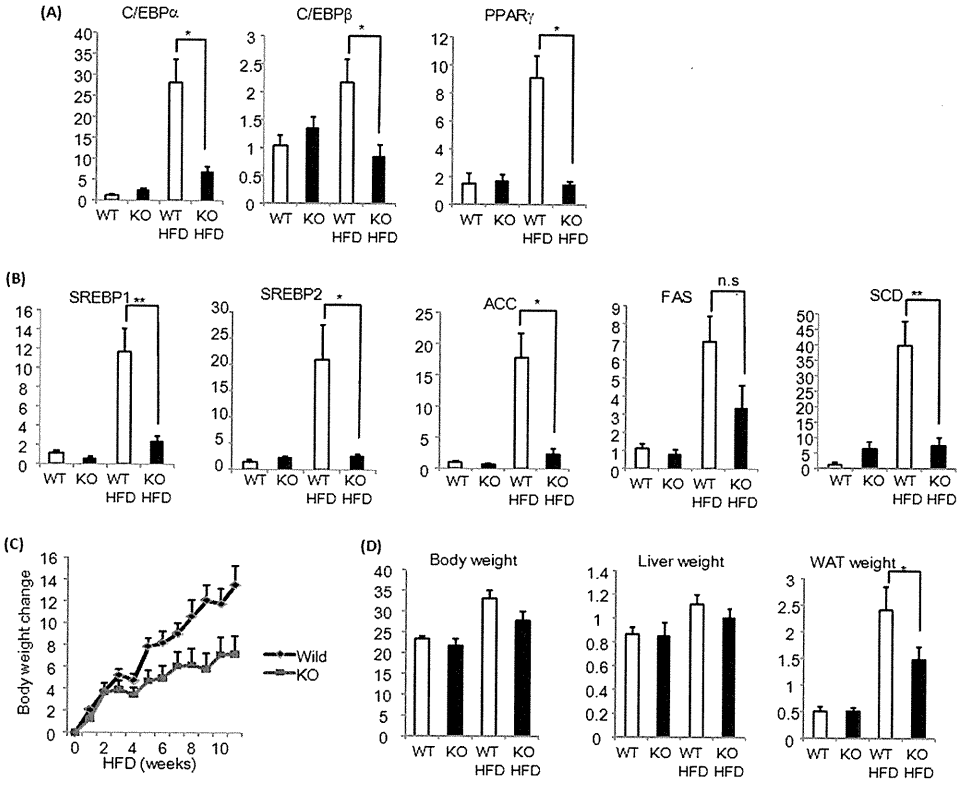

FIGURE 7. **Pin1 KO mice are resistant to HFD-induced obesity.** *A*, PPARγ, c/EBPα, and c/EBPβ mRNA levels in the adipose tissues of wild-type or Pin1 KO mice, fed a control diet or HFD for 4 weeks, were determined. *B*, SREBP1, SREBP2, ACC, FAS, and SCD mRNA levels in adipose tissues from wild-type or Pin1 KO mice, fed a control or HFD for 4 weeks, were determined by real-time PCR. *C*, weight gain after HFD feeding was compared between wild-type and Pin1 KO mice. *D*, the weights of the liver and adipose tissue were compared between wild-type and Pin1 KO mice, which had been fed either a control diet or HFD for 4 weeks. *ACC*, acetyl-CoA carboxylase; *FAS*, fatty acid synthase; *SCD*, stearoyl-CoA-desaturase.

genesis as Pin1 KO mice were clearly resistant to HFD-induced obesity.

DISCUSSION

Pin1 amounts increased according to nutrient state, as shown by marked elevation on a high-fat as compared with a normal diet. The Pin1 level was also higher in the fed than in the fasted state (19). Whereas previous studies have shown that Pin1 expression generally correlates with cell proliferative potential in normal tissues (7, 12) and is further up-regulated in many human cancers (30, 31), our findings are the first suggesting a relationship between Pin1 protein and nutrient conditions.

We also demonstrated that Pin1 is a positive regulator of insulin signaling via enhanced insulin-induced IRS-1 phosphorylation, based on a data series obtained using *in vitro* and *in vivo* overexpression of Pin1, gene silencing, a specific inhibitor, and Pin1 KO mice. The principal insulin receptor substrates, IRS-protein family members such as IRS-1 and IRS-2, adaptor proteins from the activated insulin receptor, are tyrosine-phosphorylated and thereby activate phosphatidylinositol 3-kinase/Akt. Pin1 binds to the Ser-434-containing motif of IRS-1, which is in the SAIN domain, via its WW domain. Because the SAIN domain reportedly plays an important role in the association with the insulin receptor (21, 22), it is speculated that Pin1 modifies the conformation of the SAIN domain and thereby enhances IRS-1 tyrosine phosphorylation by the insulin receptor. Similar enhanced phosphorylation of signal transduction protein via association with Pin1 has been reported for STAT3 (32).

Regarding the downstream signaling from the insulin receptor, the phosphatidylinositol 3-kinase/Akt pathway activation is essential for almost all insulin-induced glucose and lipid metabolism activities, *e.g.* glucose uptake, glycogen synthesis, suppression of glucose output, and triglyceride synthesis. Thus, in the muscles of Pin1 KO mice showing impaired Akt activation, glucose incorporation into muscle with insulin stimulation was decreased.

Insulin-induced phosphatidylinositol 3-kinase/Akt activations also play a role in adipogenesis (25, 33). It was shown that Pin1-deficient preadipocytes clearly fail to differentiate into adipocytes. This suppression was accompanied by insufficient inductions of PPARγ, c/EBPα, and c/EBPβ. On the other hand, overexpression of PPARγ reversed the Pin1 siRNA-induced suppression of adipose differentiation. Although the molecular mechanisms underlying insulin-induced induction of adipogenic genes has yet to be fully elucidated, previous reports have shown the essential action of SREBPs for adipogenesis to probably be via regulation of its downstream PPARγ (34, 35). Indeed, in adipose tissue from Pin1 KO mice, SREBPs and downstream gene expressions were decreased. These observations indicate that, as a consequence of impaired adipose differentiation, Pin1 KO mice are resistant to HFD-induced obesity.

Based on our data series, we can speculate as to the physiological significance of Pin1 with respect to metabolic regula-

Downloaded from www.jbc.org at TOHOKU UNIVERSITY, on April 18, 2012

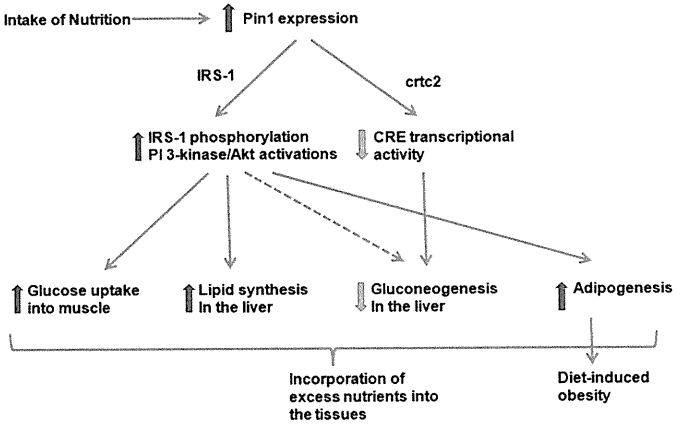

FIGURE 8. **Schema show the role of Pin1 in glucose and lipid metabolism in response to nutrient intakes.**

tion. When nutrients enter the body, excess glucose, lipids, and amino acids are stored mainly in the liver, muscle, and adipose tissue. Although insulin is the critical hormone for this process, we consider Pin1 to be involved in the mechanisms enhancing insulin sensitivity in peripheral tissues. Increased Pin1 expression functions to increase insulin sensitivity, thereby maintaining homeostasis in response to food or excess nutrient intake. Intriguingly, Pin1 enhances the signal from IRS-1 but not that from IRS-2. Although IRS-2 bound to Pin1 when both were overexpressed in HepG2 cells (supplemental Fig. 3), no association of endogenous IRS-2 and Pin1 was detected (data not shown). Thus, it is likely that IRS-2 associates with Pin1 far less efficiently than does IRS-1, which might account for the different effects of Pin1 on IRS-1 and IRS-2. Although several studies have revealed different roles for IRS-1 and IRS-2 (36, 37), we speculate that selective enhancement of IRS-1 signaling may contribute to greater hepatic lipid synthesis, as IRS-1 phosphorylation lasts much longer than that of IRS-2. Indeed, constitutive Akt overexpression induces marked lipid accumulation in the liver with blood glucose lowering (24). Thus, increased Pin1 expression is considered to be a physiologically beneficial response to excess nutrient intake.

However, excessive energy intake eventually causes fatty liver and obesity, which lead to the development of metabolic syndrome. In this condition, several kinases including mammalian target of rapamycin (mTOR), inhibitory κB kinase β, c-Jun N-terminal kinase, extracellular signal regulated kinase, and S6 kinase, induce the phosphorylations of serine 307, 302 and 612 of IRS-1, leading to reduced insulin-induced IRS-1 tyrosine phosphorylations and thereby contributing to insulin resistance (38–43). Thus, the efficiency of IRS-1 tyrosine phosphorylations appears to be up-regulated by increased Pin1 association and down-regulated by the aforementioned multiple serine phosphorylations. We speculate that both phenomena take place under conditions of energy excess, but when prolonged, the latter down-regulating mechanism becomes dominant.

In conclusion, we have demonstrated the important role of Pin1 as a positive modulator of insulin signaling as well as an inducer of obesity. Thus, Pin1 might be regarded as somewhat of a double-edged sword in that it increases insulin sensitivity but also promotes obesity (Fig. 8). However, suppression of Pin1 activity specifically in adipocytes might be a novel preventive treatment for obesity. Otherwise, if hepatic lipid accumulation is not severe, agents increasing Pin1 expression or enzymatic activity, *i.e.* targeting Pin1, may hold promise for treating Type 2 diabetes mellitus by improving hepatic insulin sensitivity.

REFERENCES

1. Fischer, G., Wittmann-Liebold, B., Lang, K., Kiefhaber, T., and Schmid, F. X. (1989) *Nature* **337,** 476–478
2. Liu, J., Farmer, J. D., Jr., Lane, W. S., Friedman, J., Weissman, I., and Schreiber, S. L. (1991) *Cell* **66,** 807–815
3. Choi, J., Chen, J., Schreiber, S. L., and Clardy, J. (1996) *Science* **273,** 239–242
4. Loewith, R., Jacinto, E., Wullschleger, S., Lorberg, A., Crespo, J. L., Bonenfant, D., Oppliger, W., Jenoe, P., and Hall, M. N. (2002) *Mol. Cell* **10,** 457–468
5. Schreiber, S. L. (1991) *Science* **251,** 283–287
6. Kunz, J., and Hall, M. N. (1993) *Trends Biochem. Sci.* **18,** 334–338
7. Lu, K. P., Hanes, S. D., and Hunter, T. (1996) *Nature* **380,** 544–547
8. Wulf, G., Finn, G., Suizu, F., and Lu, K. P. (2005) *Nat. Cell Biol.* **7,** 435–441
9. Lu, K. P., and Zhou, X. Z. (2007) *Nat. Rev. Mol. Cell Biol.* **8,** 904–916
10. Takahashi, K., Uchida, C., Shin, R. W., Shimazaki, K., and Uchida, T. (2008) *Cell. Mol. Life Sci.* **65,** 359–375
11. Zhou, X. Z., Kops, O., Werner, A., Lu, P. J., Shen, M., Stoller, G., Küllertz, G., Stark, M., Fischer, G., and Lu, K. P. (2000) *Mol. Cell* **6,** 873–883
12. Winkler, K. E., Swenson, K. I., Kornbluth, S., and Means, A. R. (2000) *Science* **287,** 1644–1647
13. Zacchi, P., Gostissa, M., Uchida, T., Salvagno, C., Avolio, F., Volinia, S., Ronai, Z., Blandino, G., Schneider, C., and Del Sal, G. (2002) *Nature* **419,** 853–857
14. Zheng, H., You, H., Zhou, X. Z., Murray, S. A., Uchida, T., Wulf, G., Gu, L., Tang, X., Lu, K. P., and Xiao, Z. X. (2002) *Nature* **419,** 849–853
15. Lu, P. J., Wulf, G., Zhou, X. Z., Davies, P., and Lu, K. P. (1999) *Nature* **399,** 784–788
16. Pastorino, L., Sun, A., Lu, P. J., Zhou, X. Z., Balastik, M., Finn, G., Wulf, G., Lim, J., Li, S. H., Li, X., Xia, W., Nicholson, L. K., and Lu, K. P. (2006) *Nature* **440,** 528–534
17. Liou, Y. C., Sun, A., Ryo, A., Zhou, X. Z., Yu, Z. X., Huang, H. K., Uchida, T., Bronson, R., Bing, G., Li, X., Hunter, T., and Lu, K. P. (2003) *Nature* **424,** 556–561
18. Nakatsu, Y., Sakoda, H., Kushiyama, A., Ono, H., Fujishiro, M., Horike, N., Yoneda, M., Ohno, H., Tsuchiya, Y., Kamata, H., Tahara, H., Isobe, T., Nishimura, F., Katagiri, H., Oka, Y., Fukushima, T., Takahashi, S., Kurihara, H., Uchida, T., and Asano, T. (2010) *J. Biol. Chem.* **285,** 33018–33027
19. Ichimura, T., Yamamura, H., Sasamoto, K., Tominaga, Y., Taoka, M., Kakiuchi, K., Shinkawa, T., Takahashi, N., Shimada, S., and Isobe, T. (2005) *J. Biol. Chem.* **280,** 13187–13194
20. Fujimori, F., Takahashi, K., Uchida, C., and Uchida, T. (1999) *Biochem. Biophys. Res. Commun.* **265,** 658–663
21. Hennig, L., Christner, C., Kipping, M., Schelbert, B., Rücknagel, K. P., Grabley, S., Küllertz, G., and Fischer, G. (1998) *Biochemistry* **37,** 5953–5960
22. Gustafson, T. A., He, W., Craparo, A., Schaub, CD., and O'Neill, T. J. (1995) *Mol. Cell. Biol.* **15,** 2500–2508
23. Yenush, L., Makati, K. J., Smith-Hall, J., Ishibashi, O., Myers, M. G., Jr., and White, M. F. (1996) *J. Biol. Chem.* **271,** 24300–24306
24. Ono, H., Shimano, H., Katagiri, H., Yahagi, N., Sakoda, H., Onishi, Y., Anai, M., Ogihara, T., Fujishiro, M., Viana, A. Y., Fukushima, Y., Abe, M., Shojima, N., Kikuchi, M., Yamada, N., Oka, Y., and Asano, T. (2003) *Diabetes* **52,** 2905–2913
25. Kerouz, N. J., Hörsch, D., Pons, S., and Kahn, C. R. (1997) *J. Clin. Invest.* **100,** 3164–3172
26. Nakae, J., Kitamura, T., Kitamura, Y., Biggs, W. H., 3rd, Arden, K. C., and Accili, D. (2003) *Dev. Cell* **4,** 119–129
27. Umek, R. M., Friedman, A. D., and McKnight, S. L. (1991) *Science* **251,** 288–292

Downloaded from www.jbc.org at TOHOKU UNIVERSITY, on April 18, 2012

28. Tanaka, T., Yoshida, N., Kishimoto, T., and Akira, S. (1997) *EMBO J.* **16,** 7432–7443
29. Spiegelman, B. M. (1998) *Diabetes* **47,** 507–514
30. Ryo, A., Nakamura, M., Wulf, G., Liou, Y. C., and Lu, K. P. (2001) *Nat. Cell Biol.* **3,** 793–801
31. Wulf, G. M., Ryo, A., Wulf, G. G., Lee, S. W., Niu, T., Petkova, V., and Lu, K. P. (2001) *EMBO J.* **20,** 3459–3472
32. Lufei, C., Koh, T. H., Uchida, T., and Cao, X. (2007) *Oncogene* **26,** 7656–7664
33. Rosen, E. D., and MacDougald, O. A. (2006) *Nat. Rev. Mol. Cell Biol.* **7,** 885–896
34. Tontonoz, P., Kim, J. B., Graves, R. A., and Spiegelman, B. M. (1993) *Mol. Cell. Biol.* **13,** 4753–4759
35. Jiang, L., Wang, Q., Yu, Y., Zhao, F., Huang, P., Zeng, R., Qi, R. Z., Li, W., and Liu, Y. (2009) *PLoS One* **4,** e6884
36. Withers, D. J., Gutierrez, J. S., Towery, H., Burks, D. J., Ren, J. M., Previs, S., Zhang, Y., Bernal, D., Pons, S., Shulman, G. I., Bonner-Weir, S., and White, M. F. (1998) *Nature* **391,** 900–904
37. Taniguchi, C. M., Emanuelli, B., and Kahn, C. R. (2006) *Nat. Rev. Mol. Cell Biol.* **7,** 85–96
38. Hotamisligil, G. S., Peraldi, P., Budavari, A., Ellis, R., White, M. F., and Spiegelman, B. M. (1996) *Science* **271,** 665–668
39. Hirosumi, J., Tuncman, G., Chang, L., Görgün, C. Z., Uysal, K. T., Maeda, K., Karin, M., and Hotamisligil, G. S. (2002) *Nature* **420,** 333–336
40. Pirola, L., Johnston, A. M., and Van Obberghen, E. (2004) *Diabetologia* **47,** 170–184
41. Werner, E. D., Lee, J., Hansen, L., Yuan, M., and Shoelson, S. E. (2004) *J. Biol. Chem.* **279,** 35298–35305
42. Ozcan, U., Yilmaz, E., Ozcan, L., Furuhashi, M., Vaillancourt, E., Smith, R. O., Görgün, C. Z., and Hotamisligil, G. S. (2006) *Science* **313,** 1137–1140
43. Morino, K., Neschen, S., Bilz, S., Sono, S., Tsirigotis, D., Reznick, R. M., Moore, I., Nagai, Y., Samuel, V., Sebastian, D., White, M., Philbrick, W., and Shulman, G. I. (2008) *Diabetes* **57,** 2644–2651

Downloaded from www.jbc.org at TOHOKU UNIVERSITY, on April 18, 2012

Increased Systemic Glucose Tolerance with Increased Muscle Glucose Uptake in Transgenic Mice Overexpressing RXRγ in Skeletal Muscle

Satoshi Sugita[1], Yasutomi Kamei[1]*, Fumiko Akaike[1,2], Takayoshi Suganami[1], Sayaka Kanai[1], Maki Hattori[1,2], Yasuko Manabe[3], Nobuharu Fujii[3], Takako Takai-Igarashi[4], Miki Tadaishi[5,6], Jun-Ichiro Oka[2], Hiroyuki Aburatani[7], Tetsuya Yamada[8], Hideki Katagiri[8], Saori Kakehi[9], Yoshifumi Tamura[9,10], Hideo Kubo[11], Kenichi Nishida[11], Shinji Miura[5], Osamu Ezaki[5], Yoshihiro Ogawa[1,12]

1 Department of Molecular Medicine and Metabolism, Medical Research Institute, Tokyo Medical and Dental University, Tokyo, Japan, **2** Laboratory of Pharmacology, Faculty of Pharmaceutical Sciences, Tokyo University of Science, Chiba, Japan, **3** Graduate School of Human Health Sciences, Tokyo Metropolitan University, Tokyo, Japan, **4** Department of Bioinformatics, Graduate School of Biomedical Science, Tokyo Medical and Dental University, Tokyo, Japan, **5** Nutritional Science Program, National Institute of Health and Nutrition, Tokyo, Japan, **6** Department of Nutritional Science, Faculty of Applied Bioscience, Tokyo University of Agriculture, Tokyo, Japan, **7** Research Center for Advanced Science and Technology, University of Tokyo, Tokyo, Japan, **8** Department of Metabolic Diseases, Center for Metabolic Diseases, Tohoku University Graduate School of Medicine, Miyagi, Japan, **9** Department of Medicine, Metabolism and Endocrinology, School of Medicine, Juntendo University, Tokyo, Japan, **10** Sportology Center, Juntendo University, Tokyo, Japan, **11** Daiichi-Sankyo Co., Ltd., Tokyo, Japan, **12** Global Center of Excellence Program, International Research Center for Molecular Science in Tooth and Bone Diseases, Medical Research Institute, Tokyo Medical and Dental University, Tokyo, Japan

Abstract

Background: Retinoid X receptor (RXR) γ is a nuclear receptor-type transcription factor expressed mostly in skeletal muscle, and regulated by nutritional conditions. Previously, we established transgenic mice overexpressing RXRγ in skeletal muscle (RXRγ mice), which showed lower blood glucose than the control mice. Here we investigated their glucose metabolism.

Methodology/Principal Findings: RXRγ mice were subjected to glucose and insulin tolerance tests, and glucose transporter expression levels, hyperinsulinemic-euglycemic clamp and glucose uptake were analyzed. Microarray and bioinformatics analyses were done. The glucose tolerance test revealed higher glucose disposal in RXRγ mice than in control mice, but insulin tolerance test revealed no difference in the insulin-induced hypoglycemic response. In the hyperinsulinemic-euglycemic clamp study, the basal glucose disposal rate was higher in RXRγ mice than in control mice, indicating an insulin-independent increase in glucose uptake. There was no difference in the rate of glucose infusion needed to maintain euglycemia (glucose infusion rate) between the RXRγ and control mice, which is consistent with the result of the insulin tolerance test. Skeletal muscle from RXRγ mice showed increased Glut1 expression, with increased glucose uptake, in an insulin-independent manner. Moreover, we performed *in vivo* luciferase reporter analysis using *Glut1* promoter (*Glut1*-Luc). Combination of RXRγ and PPARδ resulted in an increase in *Glut1*-Luc activity in skeletal muscle *in vivo*. Microarray data showed that RXRγ overexpression increased a diverse set of genes, including glucose metabolism genes, whose promoter contained putative PPAR-binding motifs.

Conclusions/Significance: Systemic glucose metabolism was increased in transgenic mice overexpressing RXRγ. The enhanced glucose tolerance in RXRγ mice may be mediated at least in part by increased Glut1 in skeletal muscle. These results show the importance of skeletal muscle gene regulation in systemic glucose metabolism. Increasing RXRγ expression may be a novel therapeutic strategy against type 2 diabetes.

Citation: Sugita S, Kamei Y, Akaike F, Suganami T, Kanai S, et al. (2011) Increased Systemic Glucose Tolerance with Increased Muscle Glucose Uptake in Transgenic Mice Overexpressing RXRγ in Skeletal Muscle. PLoS ONE 6(5): e20467. doi:10.1371/journal.pone.0020467

Editor: Massimo Federici, University of Tor Vergata, Italy

Received March 15, 2011; **Accepted** April 26, 2011; **Published** May 31, 2011

Copyright: © 2011 Sugita et al. This is an open-access article distributed under the terms of the Creative Commons Attribution License, which permits unrestricted use, distribution, and reproduction in any medium, provided the original author and source are credited.

Funding: This work was supported in part by a Grant-in-Aid for scientific research KAKENHI from the Japanese Ministry of Education, Culture, Sports, Science and Technology (MEXT, Tokyo, Japan), research grants from the Japanese Ministry of Health, Labor and Welfare, and by the joint research program of the Institute for Molecular and Cellular Regulation, Gunma University. S. Sugita is a Research Fellow of the Japan Society for the Promotion of Science. The funders had no role in study design, data collection and analysis, decision to publish, or preparation of the manuscript.

Competing Interests: HK and KN are currently employed by the commercial company Daiichi-Sankyo Co., Ltd. HK and KN were non-commercially involved in this study. This does not alter the authors' adherence to all the PLoS ONE policies on sharing data and materials. Therefore, HK and KN do not have competing interests to disclose.

* E-mail: kamei.mmm@mri.tmd.ac.jp

Introduction

The skeletal muscle, known as the largest organ in the human body, plays an important role in exercise, energy expenditure, and glucose metabolism. It is a major site of glucose disposal [1,2]. In type 2 diabetic subjects, glucose uptake in the skeletal muscle is impaired [2]. Blood glucose is taken up by the skeletal muscle via insulin-dependent and independent glucose transporters (Glut4